bioRxiv preprint doi: https://doi.org/10.1101/008367; this version posted June 22, 2016. The copyright holder for this preprint (which was not certified by peer review) is the author/funder, who has granted bioRxiv a license to display the preprint in perpetuity. It is made available under aCC-BY 4.0 International license.

Modeling human population separation history using physically phased genomes

Shiya Song[1], Elzbieta Sliwerska[2], Sarah Emery[2], Jeffrey M. Kidd*[1,2]
[1]Department of Computational Medicine and Bioinformatics
[2]Department of Human Genetics
University of Michigan Medical School
Ann Arbor, Michigan, USA

* Correspondence to J.M.K at jmkidd@umich.edu

Running title: Split-time estimation using physically phased genomes

Keywords
Fosmid pool sequencing, haplotype, population split-time, PSMC, MSMC, approximate Bayesian computation

bioRxiv preprint doi: https://doi.org/10.1101/008367; this version posted June 22, 2016. The copyright holder for this preprint (which was not certified by peer review) is the author/funder, who has granted bioRxiv a license to display the preprint in perpetuity. It is made available under aCC-BY 4.0 International license.

Abstract

Phased haplotype sequences are a key component in many population genetic analyses since variation in haplotypes reflects the action of recombination, selection, and changes in population size. In humans, haplotypes are typically estimated from unphased sequence or genotyping data using statistical models applied to large reference panels. To assess the importance of correct haplotype phase on population history inference, we performed fosmid pool sequencing and resolved phased haplotypes of five individuals from diverse African populations (including Yoruba, Esan, Gambia, Massai and Mende). We physically phased 98% of heterozygous SNPs into haplotype-resolved blocks, obtaining a block N50 of 1 Mbp. We combined these data with additional phased genomes from San, Mbuti, Gujarati and CEPH European populations and analyzed population size and separation history using the Pairwise Sequentially Markovian Coalescent (PSMC) and Multiple Sequentially Markovian Coalescent (MSMC) models. We find that statistically phased haplotypes yield an earlier split-time estimation compared with experimentally phased haplotypes. To better interpret patterns of cross-population coalescence, we implemented an approximate Bayesian computation (ABC) approach to estimate population split times and migration rates by fitting the distribution of coalescent times inferred between two haplotypes, one from each population, to a standard Isolation-with-Migration model. We inferred that the separation between hunter-gather populations and other populations happened around 120,000 to 140,000 years ago with gene flow continuing until 30,000 to 40,000 years ago; separation between west African and out of African populations happened around 70,000 to 80,000 years ago, while the separation between Massai and out of African populations happened around 50,000 years ago.

bioRxiv preprint doi: https://doi.org/10.1101/008367; this version posted June 22, 2016. The copyright holder for this preprint (which was not certified by peer review) is the author/funder, who has granted bioRxiv a license to display the preprint in perpetuity. It is made available under aCC-BY 4.0 International license.

Introduction

Haplotypes contain rich information about population history and are shaped by population size, natural selection, and recombination (VEERAMAH and HAMMER 2014; SCHRAIBER and AKEY 2015). Due to historic recombination events there are hundreds of thousands of pairs of loci along a chromosome that have distinct histories. Recent methodological advances permit the estimation of a detailed population demographic history from a single or several whole genome sequences based on the distribution of coalescent times across the genome. For example, Li and Durbin (LI and DURBIN 2011) developed the Pairwise Sequentially Markovian Coalescent model (PSMC) to reconstruct the distribution of the time since the most recent common ancestor (TMRCA) between the two alleles of an individual and infer population size changes over time. Typically, these TMRCA values are calculated using the two haploid genomes that compose the diploid genome of a single sample (LI and DURBIN 2011). When PSMC is applied to two haplotypes obtained from different populations, the inferred TMRCA distribution is informative about the timing of population splits since the time after which nearly no coalescence events occur is a good estimate for the population split time. One key question regarding human population history is the timing of population splits and the dynamics of separation between Africans and non-Africans, which has a great influence on modern genetic diversity. Li and Durbin (LI and DURBIN 2011) paired X chromosomes from African and non-African males and suggested that the two groups remained as one population until 60-80 kyrs ago with substantial genetic exchange up until 20-40 kyrs ago (assuming a mutation rate of 2.5×10^{-8} bp per generation and 25 years as generation time, estimates which approximately double when assuming a mutation rate 1.25×10^{-8} bp per generation and 30 years as generation time (SCHIFFELS and DURBIN 2014)). Subsequently, PSMC applied to pseudo-diploid sequences was used to date the divergence time between non-human primate subspecies (PRADO-MARTINEZ *et al.* 2013). However, PSMC curves themselves provide only a qualitative measure of population separation and estimating split times is complicated by the presence of migration (PRITCHARD 2011).

MSMC (SCHIFFELS and DURBIN 2014) extends PSMC to multiple individuals, focusing on the first coalescence event for any pair of haplotypes. With multiple haplotypes from different populations, MSMC calculates the ratio between cross-population and within-population coalescence rates, termed the 'relative cross coalescence rate', a value reflecting population separation history. Schiffels et al. (SCHIFFELS and DURBIN 2014) applied MSMC on statistically phased genomes (two or four haplotypes per population) and suggested that African and non-African populations exhibited a slow, gradual separation beginning earlier than 200,000 years ago

bioRxiv preprint doi: https://doi.org/10.1101/008367; this version posted June 22, 2016. The copyright holder for this preprint (which was not certified by peer review) is the author/funder, who has granted bioRxiv a license to display the preprint in perpetuity. It is made available under aCC-BY 4.0 International license.

and lasting until about 40,000 years ago, while the median point of such divergence was around 60,000 – 80,000 years ago. The midpoint of the relative cross-coalescence decay curve has been used as an estimate of population separation time (TEWHEY *et al.* 2011; SCHIFFELS and DURBIN 2014). Although useful, this approach does not generate parametric estimates for population history under standard models. As none of these methods to infer population separation history were applied on physically phased genomes, it is unclear how phasing errors and missing data affect this type of analysis.

In this manuscript, we construct physically phased genomes of five individuals from diverse African populations (including Yoruba, Esan, Gambia, Massai and Mende). We reanalyzed fosmid sequencing data for individuals from the Gujarati, San and Mbuti populations and assess the ability to correctly assemble SNP haplotypes using fosmid pool sequencing and compare the resulting data with statistically phased haplotypes. We have previously compared several reconstructed haplotypes from a subset of these samples with those released by 1000 Genomes Phase III Project (CONSORTIUM 2015). In this paper, we focus on how well the existing statistical phasing software SHAPEIT (DELANEAU *et al.* 2012) performs given the available 1000 Genomes reference panel and how different reference panels perform, especially for samples from populations not represented in the panel. We further assess the impact of phasing error on MSMC's estimates of population split times using physically phased genomes vs. statistically phased genomes. Finally, we extend the current PSMC method to model population splits. We apply an approximate Bayesian computation (ABC) method to obtain posterior estimates of split time and migration rate by fitting the inferred TMRCA distribution obtained from PSMC on pseudo-diploid genomes to a standard Isolation-with-Migration model. Additionally, we assess the sensitivity of existing methods to missing data and phasing errors from statistically phased haplotypes.

Materials and Methods

Reconstructing haplotypes using fosmid pool sequencing

We performed fosmid pool sequencing and standard Illumina sequencing on individuals NA19240, HG03428, HG02799, HG03108, and NA21302, the detailed methods of which is elaborated in the 1000 Genomes Phase3 paper (CONSORTIUM 2015) (Supplemental Table 1-3). Paired end reads were aligned to the reference genome assembly (GRCh37, with the pseudoautosomal regions of the Y chromosome masked to 'N') using BWA v0.5.9-r16 (LI and DURBIN 2009). PCR duplicates were removed by Picard v1.62. Reads in regions with known

bioRxiv preprint doi: https://doi.org/10.1101/008367; this version posted June 22, 2016. The copyright holder for this preprint (which was not certified by peer review) is the author/funder, who has granted bioRxiv a license to display the preprint in perpetuity. It is made available under aCC-BY 4.0 International license.

indels were locally realigned and base quality scores were recalibrated using GATK (McKenna *et al.* 2010). We generated GVCF files (Genomic VCF) with a record for every position in the genome using GATK HaplotypeCaller v3.2-2. Variants were called using GenotypeGVCFs and filtered by applying Variant Quality Score Recalibration(VQSR) implemented in GATK to select a SNP set that included 99% of sites that intersect with the HapMap and 1000 Genomes training set. We define callable regions as sites that are within half and 2 times the average coverage and with genotype and mapping quality scores greater than 20. We kept variants that either passed VQSR filtering or were present in the 1000 Genomes Phase I reference panel, which served as the starting point for subsequent haplotype phasing. We followed the procedure described in 1000 Genomes Phase3 paper (Consortium 2015) to process fosmid sequencing data. We generated phased haplotypes from five individuals plus samples NA20847 (Kitzman *et al.* 2011), HGDP01029 and HGDP00456 (Meyer *et al.* 2012) that were published previously and obtained haplotype phased blocks using ReFHap (Duitama *et al.* 2012).

For NA19240, HG02799, HG03108 and NA21302, we used phase-determined SNPs from trio genotyping available from HapMap and AffyMetrix to guide paternal and maternal allele assignment within blocks. We determined paternal and maternal allele identity based on the majority of phased SNP assignments, then identified and corrected corrected switch errors only if the increase in MEC value (minimum error correction) was less than 50 after correction. For NA20847, HG03428, HGDP01029, and HGDP00456, phase-determined SNPs from trio data are unavailable. For these samples, we applied Prism (Kuleshov *et al.* 2014), a statistical phasing algorithm designed to assemble local blocks into long global haplotype contigs. This method is an extension to the Li and Stephens's model (Li and Stephens 2003) that utilizes a reference panel of phased haplotypes and a genetic map of the genome with an additional parameter representing the phase of each block in the hidden Markov model to enforce the locally phased structure at the global phasing level. We grouped local blocks into windows with size smaller than 1Mbp and with at least 2 local blocks. Each window overlapped by 1 local block, which was used to link adjacent windows together. For sample NA12878, we directly used the phased SNP haplotypes constructed by fosmid pool sequencing from a previous study (Duitama *et al.* 2012) , downloaded from http://www.molgen.mpg.de/~genetic-variation/SIH/data, and we obtained callable regions and high-confidence SNP call sets from the sequencing results of 1000 Genomes Pilot Project (Consortium 2010) to construct full haplotypes.

MSMC analysis

bioRxiv preprint doi: https://doi.org/10.1101/008367; this version posted June 22, 2016. The copyright holder for this preprint (which was not certified by peer review) is the author/funder, who has granted bioRxiv a license to display the preprint in perpetuity. It is made available under aCC-BY 4.0 International license.

We applied the Multiple sequentially Markovian coalescent (MSMC) (SCHIFFELS and DURBIN 2014) model on four haplotypes, two haplotypes per individual each population. We used 'fixedRecombination' and 'skipAmbigous' for inference of population separation. MSMC analysis yields inferred cross-population and within-population coalescence rates. We calculated the relative cross coalescence rate (RCCR) by dividing the cross-population coalescence rate by the average of within-population coalescence rate and plotted it as a function of time. We also applied MSMC on individual diploid genomes, which is very similar to PSMC, with subtle differences due to the underlying model SMC' (MARJORAM and WALL 2006) versus SMC (MCVEAN and CARDIN 2005). In order to differentiate it from PSMC, we refer to such analysis as PSMC'.

PSMC on pseudo-diploid genome

Pairwise sequentially Markovian coalescent (PSMC) (LI and DURBIN 2011) inference was performed as previously described (LI and DURBIN 2011). PSMC builds a HMM to infer the local TMRCA based on the local density of heterozygotes. In the model, hidden states are discretized TMRCA values, and transitions represents ancestral recombination events. On autosomal data, we use the default setting with T_{max}=15, n=64, and pattern '1*4+25*2+1*4+1*6'. When applying PSMC on a pseudo-diploid genome, there are four possible configurations of the two haplotypes, namely hap1-hap1, hap1-hap2, hap2-hap1, hap2-hap2. We applied PSMC to each possible configuration and took the average of the estimates. We obtained the inferred TMRCA distribution directly from PSMC output, the fifth column representing the fraction of the genome that coalesced in an indicated TMRCA bin.

ABC analysis

We implemented an ABC framework to estimate split time and migration rate given the inferred TMRCA distribution from PSMC output. We computed the coalescence time density of two chromosomes based on the Isolation-With-Migration model (WANG and HEY 2010; HOBOLTH *et al.* 2011) and integrated coalescence time density on the 64 time intervals in which PSMC is parameterized. We use chi-square statistics calculated between the observed TMRCA distribution obtained from PSMC output and the computed one as the distance between estimates in the ABC framework.

We formulate the IM model as continuous time Markov chain (WANG and HEY 2010; HOBOLTH *et al.* 2011). The rate matrix Q is given by:

bioRxiv preprint doi: https://doi.org/10.1101/008367; this version posted June 22, 2016. The copyright holder for this preprint (which was not certified by peer review) is the author/funder, who has granted bioRxiv a license to display the preprint in perpetuity. It is made available under aCC-BY 4.0 International license.

$$Q = \begin{pmatrix} . & 2m_1 & 0 & 2/\theta_1 & 0 \\ m_2 & . & m_1 & 0 & 0 \\ 0 & 2m_2 & . & 0 & 2/\theta_2 \\ 0 & 0 & 0 & . & m_1 \\ 0 & 0 & 0 & m_2 & . \end{pmatrix},$$

where the states are S_{11}(both gene are in population 1), S_{12} (one gene is in population 1 and the other is in population 2), S_{22} (both gene are in population 2), S_1 (the genes have coalesced and the single gene is in population 1), S_2 (the genes have coalesced and the single gene is in population 1), and θ_1 and θ_2 is the scaled population sizes, and m_1 and m_2 are the migration rates. The density of coalescence time can be calculated as follows:

$$f(t) = (e^{Qt})_{S_{12}S_{11}}\left(\frac{2}{\theta_1}\right) + (e^{Qt})_{S_{12}S_{22}}\left(\frac{2}{\theta_2}\right) \; for\; t < T$$

$$f(t) = [(e^{QT})_{S_{12}S_{11}} + (e^{QT})_{S_{12}S_{12}} + (e^{QT})_{S_{12}S_{22}}] * \frac{2}{\theta_a(t)} * \exp\left(-\int_T^t \frac{2}{\theta_a(t')}dt'\right) for\; t > T$$

where T is the split time and $\theta_a(t)$ the ancestral population size. We use the ancestral population size inferred from PSMC of the pseudo-diploid genome as the ancestral population size, and use the inferred population size of each diploid genome (from PSMC) as the population size for each population after the split. For African populations, we assume constant population size after the split. For non-African populations, we assume that the population experienced a bottleneck event after the split and experienced population growth beginning 40 kyrs ago. For our ABC framework, the parameters of interests are T (split time) and m (migration rate after the split). We assumed a uniform prior for the split time and time when migration ends, and a uniform prior on migration rate in log10 scale, and applied an ABC method based on sequential Monte Carlo (TONI *et al.* 2009) (SMC) to the parameter estimation, since it can be easily run in parallel and is more efficient than an ABC rejection sampler. We drew a pool of 5000 candidate parameter values (called particles) from the prior distribution. Instead of setting the final stringent cut-off ε (if the distance between summary statistics are lower than ε, we accept it), we gradually lowered the tolerance $\varepsilon_1 > \varepsilon_2 > \varepsilon_3 >> 0$, thus the distributions gradually evolve toward the target posterior. The first pool was generated by sampling from the prior distribution. The particles that were accepted using the first threshold ε_1 were sampled by their weights and perturbed to get new particles. As the tolerance threshold lowered to the final cut-off, we obtained the target posterior distribution. In each iteration, we choose the threshold ε such that 20% of particles are accepted, achieving N=1000 accepted particles. The perturbation kernels for all parameters are uniform, K=σU(-1,1), with σ equal to 20% of the difference between maximum and minimum values. We perform three

bioRxiv preprint doi: https://doi.org/10.1101/008367; this version posted June 22, 2016. The copyright holder for this preprint (which was not certified by peer review) is the author/funder, who has granted bioRxiv a license to display the preprint in perpetuity. It is made available under aCC-BY 4.0 International license.

iterations and summarized the mean, median and 95% HPD confidence interval for each parameter. For simulations, we generated 100 30Mb sequences of two individuals representing African and European samples and having split times ranging from 60 kyrs to 150 kyrs ago, with subsequent migration until 30 kyrs ago using MaCS (CHEN *et al.* 2009).

Results

Haplotype reconstruction

We utilized RefHap to reconstruct haplotypes using fosmid pool sequencing of 8 individuals from diverse populations (NA19240 (Yoruba), HG02799 (Gambia), HG03108 (Esan), HG03428 (Mende), NA21302 (Maasai), HGDP01029 (San), HGDP00456 (Mbuti) and NA20847 (Gujarati) and obtained phased haplotypes for NA12878 (CEU) from a previous study (DUITAMA *et al.* 2012; PRÜFER *et al.* 2014). In total across all pools, each genome was covered by an average of 6-17 clones with a median sequence coverage ranging 16.9-24.8x (Supplemental Table 2). The effect of increased clone counts on phased block size is dramatic: when doubling the number of fosmid clones, the N_{50} of phased blocks tripled, achieving over 1Mbp for four of the African samples (Figure 1, Table 1).

Although SNPs within each block are phased, the relationships between blocks cannot be directly established due to the absence of linking fosmid clones. We utilized two approaches to overcome this limitation. For samples that are members of genotyped trios, we utilized SNP transmission patterns to link adjacent blocks together producing near-to-complete haplotypes, encompassing over 97% of total heterozygous SNPs for HG02799, HG03108, NA21302, and 92.7% for NA19240. Comparison with deterministically phased SNPs identified potential switch errors due to insufficient clone support within our inferred haplotypes, which we corrected prior to subsequent analysis (Table 1, Supplemental Figure 1). We find 99.66% concordance between the fosmid-phased SNPs for NA19240 and heterozygous SNPs phased based on transmission from this sequenced trio (CONSORTIUM 2010). We further compared our phased haplotypes for NA19240 to the sequence of 33 fosmid clones from the same individual (KIDD *et al.* 2008), observing differences at 5 of the 1,013 heterozygous sites (0.5%) encompassed by the 33 clones (Supplemental Table 4). In total, the aligned clones encompass 1,102,213 bp excluding alignment gaps, and have 51 single nucleotide differences in comparison with our data. If we assume that all of these differences are errors in our inferred sequences, this suggests that our haplotypes have an overall sequence error rate of less than 0.005% or a Phred (EWING and GREEN 1998) quality score greater than Q40.

bioRxiv preprint doi: https://doi.org/10.1101/008367; this version posted June 22, 2016. The copyright holder for this preprint (which was not certified by peer review) is the author/funder, who has granted bioRxiv a license to display the preprint in perpetuity. It is made available under aCC-BY 4.0 International license.

For individuals HG03428 (MSL), NA20847 (GIH), HGDP01029 (San), and HGDP00456 (Mbuti), trio data is unavailable. For these samples, we assigned 80%-98% of SNPs to a parental allele using Prism (KULESHOV *et al.* 2014), a statistical phasing algorithm designed to assemble short local blocks into longer global haplotype contigs. To evaluate how well Prism performs in this context of large haplotype-block assignment, we applied Prism to NA19240 and HG02799 and compared the assignment of local blocks with our assignment based on trio phase-determined SNPs. For NA19240, 6575 out of 13591 blocks (47.6%) were assigned differently, affecting 45.88% of total heterozygous SNPs. For HG02799, 1214 out of 2810 blocks (43.2%) were assigned differently, affecting 41.82% of total heterozygous SNPs. This results in mean inter-switch distance of 2335 kbp and mean incorrectly phased haplotype length of 1967 kbp, with a 0.03% switch error rate.

Comparison with statistical phasing

We applied SHAPEIT (DELANEAU *et al.* 2012) using either the 1000 Genomes Phase 1 reference panel(ABECASIS *et al.* 2012) (1092 individuals, 14 populations) or Phase3 reference panel(CONSORTIUM 2015) (2504 individuals, 27 populations) separately to statistically phase each individual (Supplemental Figure 2, Table 2). For haplotypes phased using the 1000 Genomes Phase 1 reference panel, the average switch error rate is 2.52%, half of which are flip errors, namely single alleles appearing on the opposite haplotype. Haplotypes phased using the Phase3 reference panel have a higher concordance rate (72.79%), longer mean length of incorrectly phased haplotype (108.0 kbp) and mean inter-switch distance (184.2 kbp), but similar levels of switch error rate (2.04%) and flip error rate (1.12%). This reflects the high accuracy of the 1000 Genomes Phase 3 release haplotypes, a result of a multi-stage phasing process that utilized a haplotype scaffold of trio-genotyped SNPs. For NA21302, HGDP01029, HGDP00456, whose populations are not included in 1000 Genomes reference panel, the level of switch errors and incorrectly phased haplotype were similar using either the Phase1 or Phase3 reference panel. For HG03428, NA20847, HGDP01029 and HDP00456, the comparisons of haplotypes are restrained to within blocks since blocks were statistically linked into long global haplotypes.

The impact of phasing error on inference using MSMC

We applied PSMC', similar to PSMC but using the SMC' framework to perform demographic inference on nine individuals from nine populations. We assumed a human mutation rate of 1.25×10^{-8} bp per generation and 30 years as generation time, although results can be easily rescaled for comparison with other estimates (KONG *et al.* 2012; SCHIFFELS and DURBIN 2014).

bioRxiv preprint doi: https://doi.org/10.1101/008367; this version posted June 22, 2016. The copyright holder for this preprint (which was not certified by peer review) is the author/funder, who has granted bioRxiv a license to display the preprint in perpetuity. It is made available under aCC-BY 4.0 International license.

Consistent with previous findings, the PSMC' curves of the nine individuals revealed that all populations shared the same two-fold increase of ancestral population size prior to 300 kyrs ago, after which the inferred population size of the African populations began to differentiate from non-African populations with all gradually experiencing an effective population size reduction (Figure 2), although we note that the simulations indicate that such shifts in PSMC curves may overestimate the timing of population size changes (LI and DURBIN 2011; PRUFER *et al.* 2014; HENN *et al.* 2015). Non-African populations experienced a ten-fold reduction of effective population size, but experienced a rapid population growth after 30 kyrs ago. Such observations were equivalent to previous PSMC analysis on diploid genomes after adjusting for differences in assumed mutation rate (LI and DURBIN 2011; MEYER *et al.* 2012; SCHIFFELS and DURBIN 2014).

The multiple sequentially Markovian coalescent (MSMC) (SCHIFFELS and DURBIN 2014) model extends PSMC to multiple individuals. MSMC estimates the relative cross population coalescence rate, which drops from one to zero as populations separate. We applied the Multiple sequentially Markovian coalescent (MSMC) model on four physically phased haplotypes, two haplotypes per individual from each population and plotted the relative cross coalescence rate as a function of time (Supplemental Figure 3), using the time when RCCR drops to 50% as an estimate of the split time (Figure 3). We noticed that the more ancient the split event, the wider the inferred time interval. A similar pattern was also observed using simulated data (Supplemental Figure 4). We also performed MSMC analysis on haplotypes inferred using SHAPEIT (triangle, Figure 3). Statistically phased haplotypes show a more recent separation time and a narrower time span, particularly for comparisons involving San or Mbuti samples.

An ABC method to infer population split time using PSMC on pseudo-diploid genomes

PSMC applied to pseudo-diploid samples also provides information on population separation history. If population splits are total and sudden, no coalescent events between populations will occur after their separation. Thus, when applying PSMC on a pseudo-diploid individual where one chromosome comes from one population and the second chromosome comes from another population, the time when the PSMC estimate of N_e goes to infinity provides an estimate for the population split time (LI and DURBIN 2011). However, the inferred PSMC curve usually increases in a step-wise manner, making it difficult to determine the exact time of split event. Subsequent migration after the split is a further confounding factor (PRITCHARD 2011).

To better interpret pseudo-diploid PSMC curves (Figure 4 and Supplemental Figure 5), we implemented an ABC framework to estimate the population split time and migration rate

bioRxiv preprint doi: https://doi.org/10.1101/008367; this version posted June 22, 2016. The copyright holder for this preprint (which was not certified by peer review) is the author/funder, who has granted bioRxiv a license to display the preprint in perpetuity. It is made available under aCC-BY 4.0 International license.

given the TMRCA distribution inferred from the PSMC output. We compared the observed TMRCA distribution with the analytical distribution determined by an Isolation-With-Migration model(WANG and HEY 2010; HOBOLTH *et al.* 2011) with the indicated values for split time and post-separation migration and applied an ABC method based on sequential Monte Carlo(TONI *et al.* 2009) (also abbreviated as ABC-SMC) to estimate the target posterior distribution of each parameter. We tested this approach using simulated data with a split time ranging from 60 kyrs to 150 kyrs ago, with subsequent migration continuing until 30 kyrs ago (Supplemental Figure 6). For each split-time, we considered three levels of symmetrical migration: 2×10^{-5}, 10×10^{-5}, 40×10^{-5}. For small levels of migration, the inferred split is quite accurate, with the mean value of the posterior distribution centered on the true value. However, for larger migration rates the inferred split-time tends to be smaller than the true value. This bias is exacerbated with subsequent iterations of ABC sampling. The magnitude of the inferred migration rate is reasonably accurate, as observed in the log10 scale.

An additional complication in the application of this method to real data is the treatment of unphased sites, which generally impact less than 10% of SNPs in each comparison (Supplemental Table 5). Using our simulations, we evaluated three methods for processing unphased SNPs: 1) randomly assigning the phase, 2) marking unphased sites along with all homozygous segments ending in an unphased heterozygous site as missing data (as recommended for MSMC) (SCHIFFELS and DURBIN 2014) and 3) marking only unphased SNPs as missing data. Even with 10% of unphased sites, the third method results in a PSMC curve similar to the original, while the first two methods give PSMC curves shifted to an earlier increased effective population size, which may result in an earlier inferred split time (Supplemental Figure 7). We therefore applied the third method to unphased SNPs in our analysis.

Inferred split times using physically phased genomes

We applied our ABC method to date the split-times among African and European populations (Figure 5, Supplemental Figure 8). We find that the San population separated from the other samples the earliest, around 120 kyrs to 140 kyrs ago, with subsequent migration rate around $10\sim15\times10^{-5}$ until 30-40 kyrs ago, an estimate that is more recent than that obtained from MSMC analysis (the median point of divergence using MSMC of San from other African populations was around 130 kyrs ago, and 160 kyrs ago with CEU population). The separation between west African and CEU populations occurred 70-80 kyrs ago with migration at a rate of $8\sim40\times10^{-5}$ until 30 kyrs ago, while Maasai separated from the CEU population around 50 kyrs ago with a greater amount of gene flow until present, with migration rate on the magnitude of 10^{-3}.

bioRxiv preprint doi: https://doi.org/10.1101/008367; this version posted June 22, 2016. The copyright holder for this preprint (which was not certified by peer review) is the author/funder, who has granted bioRxiv a license to display the preprint in perpetuity. It is made available under aCC-BY 4.0 International license.

The separation between west African and MKK population occurred around 36 kyrs to 40 kyrs ago, also with a great amount of gene flow until present, with migration rate on magnitude of 10^{-3}. The separation between CEU and GIH occurred around 36 kyrs to 38 kyrs ago, with ongoing migration on the magnitude of 10^{-3} until present. Comparisons with statistically-phased data suggest that the impact of phasing error on our PSMC-ABC method is less dramatic than for MSMC analysis, however when using haplotypes phased by SHAPEIT, a larger proportion of the genome coalesced ~50,000 years ago than when fosmid-phased haplotypes are used (Supplemental Figure 9, Supplemental Figure 10). This may result in larger amounts of inferred gene flow when using statistically phased data.

Discussion

The utility of phase-resolved genome sequence data in the interpretation of variants impacting gene expression, transcription factor binding, human disease, and genome assembly has motivated the development of multiple approaches for determining phase. Here, we focus on samples phased using fosmid-based dilution haplotyping, and analyze a diverse set of eight phase-resolved human genomes. As expected, we find that phase results improve with increasing number of sequenced clones. We also demonstrate that statistical phasing performs well using existing reference panels, particularly when the panel captures population variation form the studied individuals. Nonetheless, the resulting phase-errors are sufficient to impact inference of population history using the MSMC model. We find that the statistically phased haplotypes show a more recent inferred population split time, perhaps due to phasing bias that make haplotypes appear more similar than they truly are. This effect is particularly noticeable for comparisons involving more deeply diverged population samples that are not well-phased using existing reference panels.

Existing PSMC and MSMC approaches represent important methodological advances and have had a clear impact on the inference of population history using individual genome sequences. However, these approaches provide only a qualitative sense of population separation history. Here, we describe the fitting of a standard Isolation with Migration model to cross-population TMRCA distributions inferred from PSMC. This allows the acquisition of parameter estimates under standard models widely utilized in population genetic inference. However, as expected, multiple combination of split time and migration rate are sometimes indistinguishable, highlighting the difficulty of inferring split times with the presence of migration (PRITCHARD 2011). This is partly due to the limitations of discretizing time and the poor resolution for recent history when given two haplotypes. Additionally, we find very high levels of migration for recent

bioRxiv preprint doi: https://doi.org/10.1101/008367; this version posted June 22, 2016. The copyright holder for this preprint (which was not certified by peer review) is the author/funder, who has granted bioRxiv a license to display the preprint in perpetuity. It is made available under aCC-BY 4.0 International license.

population splits (MKK and CEU, GIH and CEU, YRI and MKK), values which might be over-estimated because of the high uncertainty for estimates of recent population history.

The split times inferred using our ABC method are generally concordant with the time when relative cross-coalescence rate dropped to 50% as inferred using MSMC, however our method provides a narrower range while quantifying the level of subsequent migration (Table 3). Utilizing this approach with fully phased haplotypes from nine populations, we provide additional estimates of key population separation in human population history. Overall, our estimates are broadly consistent with other contemporary methods (Supplemental Table 6) and our estimates are consistent with the timing of the most recent common ancestor of African and non-African mitochondrial DNA, around 78,300 years ago and the timing of the mitochondrial MRCA for all modern humans at 157,000 years ago (FU *et al.* 2013).

Similar to previous results (SCHIFFELS and DURBIN 2014), the separation history between CEU and MKK populations was different from that observed between CEU and LWK (Luhya, another east African population). Two pulses of admixture have been estimated in the ancestors of the MKK, occurring 8 and 88 generations ago ((PAGANI *et al.* 2012; PICKRELL *et al.* 2014)). Since the impact of long segments of shared ancestry due to recent admixture is unclear, we masked out regions of recent European ancestry in our MKK sample using RFMix (MAPLES *et al.* 2013) (Supplemental Figure 11) and found that the MSMC curves are not altered when recent segments of European ancestry are masked (Supplemental Figure 12). Although such ancestral masking becomes increasingly imperfect for older admixture events, this suggests that long segments of shared ancestry due to recent admixture do not explain the latter divergence of Massai population compared to other African populations and supports a more complex ancient history for the Massai.

When constructing global haplotypes for individuals without trio phasing data available, we applied Prism to statistically link blocks together. Prism was designed to link much shorter phased segments into longer blocks. When applied to our phased haplotype blocks, we found that around 40% of blocks were assigned incorrectly, resulting in switch errors every 2 Mbp. However, we found very similar MSMC curve using global haplotypes constructed by Prism with those constructed with trio phasing data (Supplemental Figure 13), indicating long switch errors have little effect on such inference. This is reassuring since we are using Prism to construct global haplotypes for four individuals; but, the inferred split times involving the San and Mbuti populations are still likely underestimated.

Our results indicate that the separation of the studied human populations was a gradual event, with substantial genetic exchange continuing after an initial split, a finding consistent with

bioRxiv preprint doi: https://doi.org/10.1101/008367; this version posted June 22, 2016. The copyright holder for this preprint (which was not certified by peer review) is the author/funder, who has granted bioRxiv a license to display the preprint in perpetuity. It is made available under aCC-BY 4.0 International license.

hypotheses of long-standing ancient population structure in Africa (reviewed in (HARDING and MCVEAN 2004; HENN *et al.* 2012)). We provide a comparison of PSMC and MSMC based methods with other contemporary methods on inferring population separation history and our results emphasize the importance of accurately phased haplotypes on MSMC analyses, especially for more ancient splits.

Acknowledgments

We thank Jacob Kitzman, Peedikayil Thomas, Jeffrey W. Innis, and the University of Michigan DNA Sequencing Core Facility for guidance on fosmid pool construction and sequencing.

Web Resources

The reconstructed haplotypes are available for download from DataDyrad under accessions XXX.

References

ABECASIS, G. R., A. AUTON, L. D. BROOKS, M. A. DEPRISTO, R. M. DURBIN *et al.*, 2012 An integrated map of genetic variation from 1,092 human genomes. Nature **491:** 56-65.

CHEN, G. K., P. MARJORAM and J. D. WALL, 2009 Fast and flexible simulation of DNA sequence data. Genome research **19:** 136-142.

CONSORTIUM, G. P., 2010 A map of human genome variation from population-scale sequencing. Nature **467:** 1061-1073.

CONSORTIUM, G. P., 2015 A global reference for human genetic variation. Nature **526:** 68-74.

DELANEAU, O., J. MARCHINI and J.-F. ZAGURY, 2012 A linear complexity phasing method for thousands of genomes. Nature methods **9:** 179-181.

DUITAMA, J., G. K. MCEWEN, T. HUEBSCH, S. PALCZEWSKI, S. SCHULZ *et al.*, 2012 Fosmid-based whole genome haplotyping of a HapMap trio child: evaluation of Single Individual Haplotyping techniques. Nucleic Acids Res **40:** 2041-2053.

EWING, B., and P. GREEN, 1998 Base-calling of automated sequencer traces using phred. II. Error probabilities. Genome Res **8:** 186-194.

FU, Q., A. MITTNIK, P. L. JOHNSON, K. BOS, M. LARI *et al.*, 2013 A revised timescale for human evolution based on ancient mitochondrial genomes. Current Biology **23:** 553-559.

HARDING, R. M., and G. MCVEAN, 2004 A structured ancestral population for the evolution of modern humans. Curr Opin Genet Dev **14:** 667-674.

HENN, B. M., L. R. BOTIGUE, S. PEISCHL, I. DUPANLOUP, M. LIPATOV *et al.*, 2015 Distance from sub-Saharan Africa predicts mutational load in diverse human genomes. Proceedings of the National Academy of Sciences: 201510805.

HENN, B. M., L. L. CAVALLI-SFORZA and M. W. FELDMAN, 2012 The great human expansion. Proc Natl Acad Sci U S A **109:** 17758-17764.

bioRxiv preprint doi: https://doi.org/10.1101/008367; this version posted June 22, 2016. The copyright holder for this preprint (which was not certified by peer review) is the author/funder, who has granted bioRxiv a license to display the preprint in perpetuity. It is made available under aCC-BY 4.0 International license.

HOBOLTH, A., L. N. ANDERSEN and T. MAILUND, 2011 On computing the coalescence time density in an isolation-with-migration model with few samples. Genetics **187:** 1241-1243.

KIDD, J. M., Z. CHENG, T. GRAVES, B. FULTON, R. K. WILSON *et al.*, 2008 Haplotype sorting using human fosmid clone end-sequence pairs. Genome Res **18:** 2016-2023.

KITZMAN, J. O., A. P. MACKENZIE, A. ADEY, J. B. HIATT, R. P. PATWARDHAN *et al.*, 2011 Haplotype-resolved genome sequencing of a Gujarati Indian individual. Nat Biotechnol **29:** 59-63.

KONG, A., M. L. FRIGGE, G. MASSON, S. BESENBACHER, P. SULEM *et al.*, 2012 Rate of de novo mutations and the importance of father's age to disease risk. Nature **488:** 471-475.

KULESHOV, V., D. XIE, R. CHEN, D. PUSHKAREV, Z. MA *et al.*, 2014 Whole-genome haplotyping using long reads and statistical methods. Nature biotechnology **32:** 261-266.

LI, H., and R. DURBIN, 2009 Fast and accurate short read alignment with Burrows-Wheeler transform. Bioinformatics **25:** 1754-1760.

LI, H., and R. DURBIN, 2011 Inference of human population history from individual whole-genome sequences. Nature **475:** 493-496.

LI, N., and M. STEPHENS, 2003 Modeling linkage disequilibrium and identifying recombination hotspots using single-nucleotide polymorphism data. Genetics **165:** 2213-2233.

MAPLES, B. K., S. GRAVEL, E. E. KENNY and C. D. BUSTAMANTE, 2013 RFMix: a discriminative modeling approach for rapid and robust local-ancestry inference. The American Journal of Human Genetics **93:** 278-288.

MARJORAM, P., and J. D. WALL, 2006 Fast. BMC genetics **7:** 16.

MCKENNA, A., M. HANNA, E. BANKS, A. SIVACHENKO, K. CIBULSKIS *et al.*, 2010 The Genome Analysis Toolkit: a MapReduce framework for analyzing next-generation DNA sequencing data. Genome Res **20:** 1297-1303.

MCVEAN, G. A., and N. J. CARDIN, 2005 Approximating the coalescent with recombination. Philos Trans R Soc Lond B Biol Sci **360:** 1387-1393.

MEYER, M., M. KIRCHER, M.-T. GANSAUGE, H. LI, F. RACIMO *et al.*, 2012 A high-coverage genome sequence from an archaic Denisovan individual. Science **338:** 222-226.

PAGANI, L., T. KIVISILD, A. TAREKEGN, R. EKONG, C. PLASTER *et al.*, 2012 Ethiopian genetic diversity reveals linguistic stratification and complex influences on the Ethiopian gene pool. The American Journal of Human Genetics **91:** 83-96.

PICKRELL, J. K., N. PATTERSON, P.-R. LOH, M. LIPSON, B. BERGER *et al.*, 2014 Ancient west Eurasian ancestry in southern and eastern Africa. Proceedings of the National Academy of Sciences **111:** 2632-2637.

PRADO-MARTINEZ, J., P. H. SUDMANT, J. M. KIDD, H. LI, J. L. KELLEY *et al.*, 2013 Great ape genetic diversity and population history. Nature **499:** 471-475.

PRITCHARD, J. K., 2011 Whole-genome sequencing data offer insights into human demography. Nature genetics **43:** 923-925.

PRÜFER, K., F. RACIMO, N. PATTERSON, F. JAY, S. SANKARARAMAN *et al.*, 2014 The complete genome sequence of a Neanderthal from the Altai Mountains. Nature **505:** 43-49.

PRUFER, K., F. RACIMO, N. PATTERSON, F. JAY, S. SANKARARAMAN *et al.*, 2014 The complete genome sequence of a Neanderthal from the Altai Mountains. Nature **505:** 43-49.

SCHIFFELS, S., and R. DURBIN, 2014 Inferring human population size and separation history from multiple genome sequences. Nat Genet **advance online publication**.

SCHRAIBER, J. G., and J. M. AKEY, 2015 Methods and models for unravelling human evolutionary history. Nature Reviews Genetics.

TEWHEY, R., V. BANSAL, A. TORKAMANI, E. J. TOPOL and N. J. SCHORK, 2011 The importance of phase information for human genomics. Nature Reviews Genetics **12:** 215-223.

bioRxiv preprint doi: https://doi.org/10.1101/008367; this version posted June 22, 2016. The copyright holder for this preprint (which was not certified by peer review) is the author/funder, who has granted bioRxiv a license to display the preprint in perpetuity. It is made available under aCC-BY 4.0 International license.

TONI, T., D. WELCH, N. STRELKOWA, A. IPSEN and M. P. STUMPF, 2009 Approximate Bayesian computation scheme for parameter inference and model selection in dynamical systems. Journal of the Royal Society Interface **6:** 187-202.

VEERAMAH, K. R., and M. F. HAMMER, 2014 The impact of whole-genome sequencing on the reconstruction of human population history. Nature Reviews Genetics **15:** 149-162.

WANG, Y., and J. HEY, 2010 Estimating divergence parameters with small samples from a large number of loci. Genetics **184:** 363-379.

bioRxiv preprint doi: https://doi.org/10.1101/008367; this version posted June 22, 2016. The copyright holder for this preprint (which was not certified by peer review) is the author/funder, who has granted bioRxiv a license to display the preprint in perpetuity. It is made available under aCC-BY 4.0 International license.

Figure Legends

Figure 1. Haplotype assembly results. The relationship of block size and the cumulative length of constructed haplotypes are plotted. Dashed lines indicate the N50 of phased blocks, the block length such that 50% of the total is represented by blocks of that size or greater.

Figure 2. PSMC' inferred population history. Population sizes inferred from the autosomes of nine individuals from nine populations are shown.

Figure 3. MSMC inferred split times. Circles or triangles represent the time when the cross-coalescence rate dropped to 50%, with lines representing the time when cross-coalescence rate reached 25% and 75%. Inferred split times were inferred using haplotypes phased by the fosmid pools approach (circle) or SHAPEIT (triangle).

Figure 4. PSMC on pseudo-diploid genomes. Population sizes inferred from combined autosomes, with one haplotype chosen from each population are shown. Plotted curves are the average results obtained from four possible global haplotype configuration, namely hap1-hap1,hap1-hap2,hap2-hap1,hap2-hap2. Haplotypes were constructed using the fosmid pool approach.

Figure 5. Split times and migration rate inferred using PSMC and ABC. We implemented ABC-SMC framework to estimate split time (A) and migration rate (B) given the inferred TMRCA distribution obtained from PSMC output. The posterior distribution of last iteration (N=1000 particles) and the mean value is shown.

Supplemental Figure 1. Illustration of ReFHap's phasing result and a switch error. Each column corresponds to a SNP position, with blue indicating the reference allele and red the alternative. The first two rows are the haplotype prediction by ReFHap, followed by four rows showing HapMap phase based on trio transmission. This is followed by 12 rows depicting clone genotypes. The last row indicates the parental allele assigned for RefHap haplotype based on HapMap phasing. In the last row, blue indicates paternal allele and red indicates maternal allele. The line with a star shows where the switch error occurred.

bioRxiv preprint doi: https://doi.org/10.1101/008367; this version posted June 22, 2016. The copyright holder for this preprint (which was not certified by peer review) is the author/funder, who has granted bioRxiv a license to display the preprint in perpetuity. It is made available under aCC-BY 4.0 International license.

Supplemental Figure 2. Illustration of the metrics used to quantify phasing errors. We illustrate switch error (green bracket), inter-switch distance (purple bracket) and length of incorrectly phased haplotypes(green bracket) when comparing test haplotypes with template haplotypes.

Supplemental Figure 3. Relative cross coalescence rate inferred using MSMC. We applied msmc on four haplotypes, two from each population. We compared the relative cross coalescence curve using physically phased haplotypes (A,B,E,F) vs haplotypes phased using SHAPEIT with 1000 Genomes Phase1 panel (C,D,G,H).

Supplemental Figure 4. Relative cross coalescence rate inferred using MSMC on simulated data. We performed simulation using MaCS (100 30M sequences for each individual) with a clean population split at 50 kyrs, 80 kyrs, 100 kyrs and 150 kyrs ago. We applied msmc on simulated sequences and plotted the relative cross coalescence curve.

Supplemental Figure 5. PSMC on pseudo-diploid genomes. Population sizes inferred from combined autosomes, one haplotype from each population are shown. Sizes are the average from 4 haplotype configuration, namely hap1-hap1,hap1-hap2,hap2-hap1,hap2-hap2. Haplotypes are constructed using fosmid pool approach.

Supplemental Figure 6. Simulation results on inferring split time and migration using the combined approach of PSMC and ABC. We tested our approach using simulated data of two individuals representing African and European population and having a split time from 60 kyrs to 150 kyrs ago, with subsequent migration until 30 kyrs ago. We tested three level of migration rate, 2×10^{-5} (low), 10×10^{-5} (middle), 40×10^{-5}(high) and plotted the posterior distribution, mean and median value of split time (estimated/true) and migration rate (log10(estimated/true)) of iteration3 and iteration4 of our ABC approach.

Supplemental Figure 7. Simulation results on different approaches to deal with unphased SNPs. We simulated sequences with different levels of unphased snps (1%, 2%, 5%, 10%) and evaluated three different methods to deal with unphased snps, 1) randomly assigning the phase (green lines), 2) marking unphased snps as missing data and removing all blocks of homozygous

bioRxiv preprint doi: https://doi.org/10.1101/008367; this version posted June 22, 2016. The copyright holder for this preprint (which was not certified by peer review) is the author/funder, who has granted bioRxiv a license to display the preprint in perpetuity. It is made available under aCC-BY 4.0 International license.

calls that ended in an unphased heterozygous site (blue) and 3) merely marking unphased snps as missing data (purple).

Supplemental Figure 8. Posterior distribution of split time and migration rate inferred using ABC. We applied ABC-SMC to infer split time and migration rate based on the inferred TMRCA distribution obtained from PSMC. For each pair of populations, we plotted the posterior distribution of split time and migration rate. The color represents chi square distance between the TMRCA distribution from the observed data and the model.

Supplemental Figure 9. TMRCA distribution inferred using PSMC. The figure shows the left tail of TMRCA distribution inferred using PSMC on pseudo-diploid individuals for comparisons involving CEU (A), MKK (B), GWD (C), San (D), and Mbuti (E). Each plot shows the TMRCA distribution inferred using haplotypes phased using fosmid data (triangle) and phased using SHAPEIT with 1000 Genomes Phase1 (circle) and Phase3 (square) reference panels.

Supplemental Figure 10. Chi-square distance between TMRCA distributions using different haplotypes . We plotted the chi-square distance between TMRCA distributions obtained using different haplotypes phased using fosmid data and phased using SHAPEIT with 1000 Genomes Phase1 (blue) and Phase3 (red) reference panels.

Supplemental Figure 11. Recent European ancestry inferred by RFMix in Massai individual NA21302. The genomic locations of European ancestry (colored blue) in Massai individual NA21302 are shown.

Supplemental Figure 12. Relative cross coalescence rate inferred using MSMC with and without masking out European ancestry from Massai individual. We applied MSMC on MKK and every other population with and without masking European ancestry from the Massai individual.

Supplemental Figure 13. Comparison of relative cross coalescence rate inferred using MSMC on fosmid haplotypes constructed by trio phasing data or by Prism. We compared

bioRxiv preprint doi: https://doi.org/10.1101/008367; this version posted June 22, 2016. The copyright holder for this preprint (which was not certified by peer review) is the author/funder, who has granted bioRxiv a license to display the preprint in perpetuity. It is made available under aCC-BY 4.0 International license.

the relative cross coalescence curve for YRI-CEU and GWD-CEU, where the global haplotypes for YRI and GWD are either constructed by trio phasing data or by Prism.

bioRxiv preprint doi: https://doi.org/10.1101/008367; this version posted June 22, 2016. The copyright holder for this preprint (which was not certified by peer review) is the author/funder, who has granted bioRxiv a license to display the preprint in perpetuity. It is made available under aCC-BY 4.0 International license.

Tables

Table 1 Phasing statistics from fosmid pool sequencing. We resolved haplotypes using fosmid pool sequencing. MEC is the number of entries to correct when resolving haplotypes. Switch errors are counted as the number of switches required to obtain the same haplotype phase when comparing inferred haplotype phase with true haplotype phase. Switch error rate is switch error normalized by number of variants for comparison. For samples labeled with *, we applied Prism to link adjacent block together.

Population	Sample	Number of Clones After Filter	Number of Blocks	N50 (kbp)	MEC value	Number of SNPs to be phased	% Phased SNPs within blocks	**Number of** blocks assigned parental allele	Percent SNPs assigned parental allele	Switch Error Count	Switch Error Corrected	Switch Error Rate
YRI	NA19240	521,783	16,334	347	37,143	2,588,454	92.94%	15,171	92.74%	586	421	0.091%
GWD	HG02799	1,141,020	5,236	1416	82,387	2,780,269	99.00%	3,041	98.38%	327	146	0.163%
ESN	HG03108	1,058,027	5,416	1294	77,499	2,756,725	99.07%	3,323	98.45%	258	115	0.127%
MKK	NA21302	892,863	6,097	1416	175,935	2,736,727	98.60%	3,751	97.96%	336	265	0.098%
MSL	HG03428*	1,424,234	4,390	1849	167,294	2,775,099	99.30%	3,549	97.90%	-	-	-
GIH	NA20847*	571,419	16,838	385	44,870	1,680,704	93.37%	13,319	90.98%	-	-	-
San	HGDP01029*	358,759	17,695	228	27,712	2,623,001	87.10%	16,516	89.15%	-	-	-
Mbuti	HGDP00456*	381,075	18,465	242	28,629	2,517,569	78.70%	17,385	81.72%	-	-	-

bioRxiv preprint doi: https://doi.org/10.1101/008367; this version posted June 22, 2016. The copyright holder for this preprint (which was not certified by peer review) is the author/funder, who has granted bioRxiv a license to display the preprint in perpetuity. It is made available under aCC-BY 4.0 International license.

Table 2 Comparison between statistical phasing. We calculated haplotype concordance, switch error rate, flip error rate, mean inter-switch distance, and mean length of incorrectly phased haplotype between haplotypes resolved by fosmid pool sequencing and haplotypes statistically phased using either the 1000 Genomes Phase1 or Phase3 reference panels. * indicates that trio data was unavailable to link blocks together and phasing comparison analysis was limited to comparisons within RefHap blocks.

Individual	Haplotype Concordance	Switch Error Rate	Flip Error Rate	Mean inter-switch distance(kbp)	Mean length of incorrectly phased haplotype(kbp)
fosmid phased haplotypes vs SHAPEIT phased haplotypes using 1000 Genomes Phase1 reference Panel					
NA19240	54.60%	1.33%	0.60%	84.6	69.6
HG02799	52.46%	1.84%	0.79%	52.2	43.3
HG03108	53.62%	1.05%	0.47%	94.1	78.8
NA12878	53.18%	0.87%	0.32%	170.0	144
NA21302	52.00%	2.32%	1.02%	43.6	37.6
HG03428*	70.01%	1.88%	0.95%	42.6	28.5
NA20847*	79.30%	1.83%	0.97%	46.5	29.5
HGDP01029*	69.83%	6.87%	3.50%	12.5	7.3
HGDP00456*	78.09%	4.68%	2.70%	16.1	8.8
Average	**62.57%**	**2.52%**	**1.26%**	**62.5**	**49.7**
fosmid phased haplotypes vs SHAPEIT phased haplotypes using 1000 Genomes Phase3 reference Panel					
NA19240	68.00%	0.33%	0.21%	480.5	293.6
HG02799	77.10%	0.63%	0.27%	296.5	124.4
HG03108	69.40%	0.42%	0.27%	346.5	208.5
NA12878	58.90%	0.67%	0.32%	264.4	204.4
NA21302	53.10%	2.44%	1.08%	41.2	32.9
HG03428*	89.70%	0.66%	0.50%	132.2	56.1
NA20847*	91.50%	1.00%	0.73%	70	36.9
HGDP01029*	69.97%	7.17%	3.77%	12	6.9
HGDP00456*	77.47%	5.08%	2.97%	14.9	8.1
Average	**72.79%**	**2.04%**	**1.12%**	**184.2**	**108.0**
Fosmid phased haplotypes: assign parental alleles using trio data vs using Prism					
NA19240	54.12%	0.05%	0.00%	1242.6	1115.0
HG02799	58.18%	0.02%	0.00%	3427.3	2821.9
Average	**56.15%**	**0.03%**	**0.00%**	**2335.0**	**1968.5**

Table 3 Posterior estimates of split time and migration rate using IM model. We report the mean, median and 95% credible intervals for the posterior distribution. Migration rate are in log10 scale. We set migration continuing to the present for recent separations.

	Split Time (in kyrs)				MigrationRrate (in $\log_{10}$ scale)				Migration End (in kyrs)			
	Mean	Median	95% lower HPD	95% higher HPD	Mean	Median	95% lower HPD	95% higher HPD	Mean	Median	95% lower HPD	95% higher HPD
YRI-CEU	73.3	72.5	70.2	81.6	-3.71	-3.70	-4.12	-3.41	27.2	30.1	6.2	38.7
MKK-CEU	53.9	53.9	52.9	55.1	-2.34	-2.22	-2.66	-2.04	-	-	-	-
GIH-CEU	37.2	37.2	36.2	38.2	-2.88	-2.87	-3.17	-2.60	-	-	-	-
San-CEU	129.5	128.8	121.3	140.9	-3.95	-3.96	-4.07	-3.83	37.2	37.1	33.4	41.5
Mbuti-CEU	117.6	116.9	103.1	139.1	-3.73	-3.73	-3.82	-3.63	34.6	34.4	30.6	39.1
YRI-MKK	38.2	38.1	36.2	40.6	-2.15	-2.16	-2.30	-2.00	-	-	-	-

bioRxiv preprint doi: https://doi.org/10.1101/008367; this version posted June 22, 2016. The copyright holder for this preprint (which was not certified by peer review) is the author/funder, who has granted bioRxiv a license to display the preprint in perpetuity. It is made available under aCC-BY 4.0 International license.

bioRxiv preprint doi: https://doi.org/10.1101/008367; this version posted June 22, 2016. The copyright holder for this preprint (which was not certified by peer review) is the author/funder, who has granted bioRxiv a license to display the preprint in perpetuity. It is made available under aCC-BY 4.0 International license.

Supplemental Table 1. Summary of population geographic information and presence in HapMap or 1000 Genomes Project.

Population	Short code	Sample ID	Geography	HapMap	1000 Genomes
Yoruba	YRI	NA19240	Yoruba in Ibadan, Nigeria	Yes	Yes, Phase1
Mende	MSL	HG03428	Mende in Sierra Leone	No	Yes, Phase3
Gambian	GWD	HG02799	Gambian in Western Division, The Gambia	No	Yes, Phase3
Esan	ESN	HG03108	Esan in Nigeria	No	Yes, Phase3
Massai	MKK	NA21302	Maasai in Kinyawa, Kenya	Yes, HapMap3	No
Gujarati	GIH	NA20847	Gujarati Indians in Houston, Texas	Yes, HapMap3	No
San	San	HGDP01029	Indigenous hunter-gatherer people of Namibia	No	No
Mubti	Mbuti	HGDP00456	Indigenous pygmy groups in the Congo region of Africa	No	No

Supplemental Table 2. Summary of clone statistics of fosmid pool sequencing.

Sample	Population	SRA Accession	Number of fosmid pools	Mean fosmids per pool	Median insert length (kbp)	Median 1kbp read depth per clone	Fosmid clone coverage of genome	Median 1kb read depth of genome
NA19240	YRI	SRS628777	288	1825	34	1.95	5.8	17.9
NA20847	GIH	SRA026360	115	4969	39	1.10	7.5	14.4
HG03428	MSL	SRS722908	440	3237	37	1.03	17.0	24.8
HG02799	GWD	SRS722940	288	3962	36	0.95	14.0	18.1
HG03108	ESN	SRS722941	288	3674	35	1.20	12.7	19.2
NA21302	MKK	SRS722942	288	3100	35	1.34	10.2	16.9
HGDP01029	San	PMID:24352235	192	1868	36	-	4.6	-
HGDP00456	Mbuti	PMID:24352235	192	1984	37	-	5.0	-

Supplemental Table 3. Summary of variant calling for whole genome sequencing.

Sample	Population	SRA Accession	Coverage	Number of Called Sites	Number of heterozygous sites pre-filter	Number of heterozygous sites post-filter
NA19240	YRI	SRS628777, SRR496444, SRR496446	20	2,397,179,422	2,991,938	2,588,454
HG02799	GWD	SRS722940	26	2,582,596,514	3,247,760	2,780,269
HG03108	ESN	SRS722941	25	2,573,126,220	3,234,813	2,756,725
HG03428	MSL	SRS722908	26	2,548,867,098	3,372,407	2,775,099
NA21302	MKK	SRS722942	26	2,588,203,996	3,176,366	2,736,727
NA20847	GIH	SRP000806, SRP048601, SRR072881	24	2,013,696,898	1,791,428	1,636,344
NA12878	CEU	1000 Genomes High coverage bam	42	2,464,361,297	-	1,843,256
HGDP01029	San	PMID:24352235	34	2,473,030,394	3,140,371	2,623,001
HGDP00456	Mbuti	PMID:24352235	24	2,481,367,128	2,936,250	2,517,569

bioRxiv preprint doi: https://doi.org/10.1101/008367; this version posted June 22, 2016. The copyright holder for this preprint (which was not certified by peer review) is the author/funder, who has granted bioRxiv a license to display the preprint in perpetuity. It is made available under aCC-BY 4.0 International license.

bioRxiv preprint doi: https://doi.org/10.1101/008367; this version posted June 22, 2016. The copyright holder for this preprint (which was not certified by peer review) is the author/funder, who has granted bioRxiv a license to display the preprint in perpetuity. It is made available under aCC-BY 4.0 International license.

Supplemental Table 4. Comparison of fosmid-resolved haplotype for NA19240 with Sanger sequenced fosmid clones. Comparison of our haplotypes with the sequence of 33 fosmid clones from the same individual that were previously sequenced using standard capillary sequencing (hap1 refers to paternal allele, hap2 refers to maternal allele). A total of 5 out of 1013 heterozygous SNP error occurred when assigning 33 clones into haplotype, an error rate of 0.5%. 51 substitution errors out of 1,102,213 bp total sequences yielded a sequence error rate of 0.005%.

Clone_Name	chr	pos1	pos2	strand	# het SNP	Het mismatch	All mismatch	Length of callable sites	error rate	haplotype assignment
AC203596	20	60332560	60367311	-	55	1	6	32288	0.018	hap2
AC208180	7	109124048	109164730	-	13	0	22	34982	0.000	hap1
AC203618	14	24625251	24665998	+	38	0	0	38494	0.000	hap1
AC203625	3	13175578	13207238	+	49	0	0	30273	0.000	hap2
AC203613	17	42388348	42422435	+	9	0	0	30723	0.000	hap2
AC209301	5	103498132	103533083	+	38	0	4	29924	0.000	hap2
AC211777	2	131597914	131644819	+	50	0	1	38297	0.000	hap2
AC207436	20	61771673	61805848	-	20	0	0	31984	0.000	hap2
AC203629	2	27532275	27572319	+	26	0	0	38173	0.000	hap1
AC203601	13	84295142	84330569	+	11	0	8	31632	0.000	hap1
AC214990	20	1835027	1870122	+	33	0	0	34441	0.000	hap2
AC203623	13	50529642	50571393	-	19	0	0	38426	0.000	hap2
AC209312	19	11076696	11117117	+	6	0	0	38301	0.000	hap1
AC204964	20	36206659	36240122	-	51	0	0	32552	0.000	hap2
AC203663	12	120664025	120704371	-	11	2	0	39060	0.182	hap1
AC203633	15	83719658	83761946	+	27	2	2	38954	0.074	hap2
AC207998	5	42518686	42548692	+	15	0	0	28690	0.000	hap1
AC204962	10	73293352	73327357	-	3	0	0	33625	0.000	hap2
AC203585	12	127683544	127718788	-	24	0	0	32465	0.000	hap1
AC207584	22	24202000	24237415	-	46	0	1	33114	0.000	hap1
AC203595	17	15129257	15154073	-	24	0	0	23449	0.000	hap1
AC204968	12	108020551	108054912	-	45	0	0	32583	0.000	hap1
AC214217	20	34745579	34780635	-	14	0	0	34239	0.000	hap1
AC203614	13	27271316	27306555	-	28	0	0	32255	0.000	hap1
AC226164	17	8937695	8978811	+	48	0	0	39232	0.000	hap2
AC203609	17	9512088	9545453	+	22	0	0	25789	0.000	hap2
AC213115	2	5679730	5713339	-	19	0	0	31868	0.000	hap1
AC210876	17	3897067	3932032	-	43	0	1	33305	0.000	hap2
AC215711	8	142371608	142412790	-	55	0	0	34903	0.000	hap2
AC207992	4	162086171	162119199	+	29	0	1	29492	0.000	hap2
AC204957	7	135193786	135227398	+	22	0	0	32251	0.000	hap2
AC209156	12	104071670	104106822	+	13	0	0	33732	0.000	hap1
AC208068	16	85067617	85102315	-	107	0	0	32717	0.000	hap2

bioRxiv preprint doi: https://doi.org/10.1101/008367; this version posted June 22, 2016. The copyright holder for this preprint (which was not certified by peer review) is the author/funder, who has granted bioRxiv a license to display the preprint in perpetuity. It is made available under aCC-BY 4.0 International license.

Supplemental Table 5. Percentage of unphased SNPs. We summarized the proportion of unphased SNPs for each population combination. For 'Shapeit' we refer to applying SHAPEIT with 1000 Genomes Phase I reference panel.

	Phasing method	Unphased	Total heterozygous	% unphased
YRI-CEU	Fosmid-Fosmid	416,956	4,123,413	10.11%
	Shapeit-Shapeit	106,327	4,123,413	2.58%
MKK-CEU	Fosmid-Fosmid	311,519	4,157,467	7.49%
	Shapeit-Shapeit	155,041	4,157,467	3.73%
GWD-CEU	Fosmid-Fosmid	302,959	4,360,333	6.95%
	Shapeit-Shapeit	118,494	4,360,333	2.72%
ESN-CEU	Fosmid-Fosmid	303,306	4,360,684	6.96%
	Shapeit-Shapeit	99,700	4,360,684	2.29%
MSL-CEU	Fosmid-Fosmid	310,165	4,329,461	7.16%
	Shapeit-Shapeit	142,952	4,329,461	3.30%
GIH-CEU	Fosmid-Fosmid	328,041	2,876,160	11.41%
	Shapeit-Shapeit	109,671	2,876,160	3.81%
YRI-MKK	Fosmid-Fosmid	210,859	4,596,417	4.59%
	Shapeit-Shapeit	168,853	4,596,417	3.67%

Supplemental Table 6. Split time estimation from previous studies. Reported estimates are adjusted by using the same mutation rate $1.25*10^{-8}$ bp/generation and generation time 30 years.

Paper	Method	Mutation	San & Others split time (kyrs)		African & Non-African split time (kyrs)		European-Asian split time (kyrs)	
			Original	Adjusted	Original	Adjusted	Original	Adjusted
Gravel et al. 2011	diffusion, AFS	mu=2.36e-08, G=25			51	115.5	23	45.2
Gronau et al. 2011	Bayesian coalescent based	HC divergence 6.5Mya, mu=2e-08	131 (127-135)	218 (214-226)	47 (44-49)	79 (74-82)	36 (34-38)	60 (57-65)
Harris et al. 2013	IBS sharing				55	85.6		
Excoffier et al, 2013	fastsimcoal2	mu=2.5e-08,G=25	65 (25-96)	156 (60-230)				
Veeramah et al. 2011	ABC	HC divergence 6 Mya, mu=2.5e-08	110 (52-187)	220 (104-374)				

bioRxiv preprint doi: https://doi.org/10.1101/008367; this version posted June 22, 2016. The copyright holder for this preprint (which was not certified by peer review) is the author/funder, who has granted bioRxiv a license to display the preprint in perpetuity. It is made available under aCC-BY 4.0 International license.

Figure 1

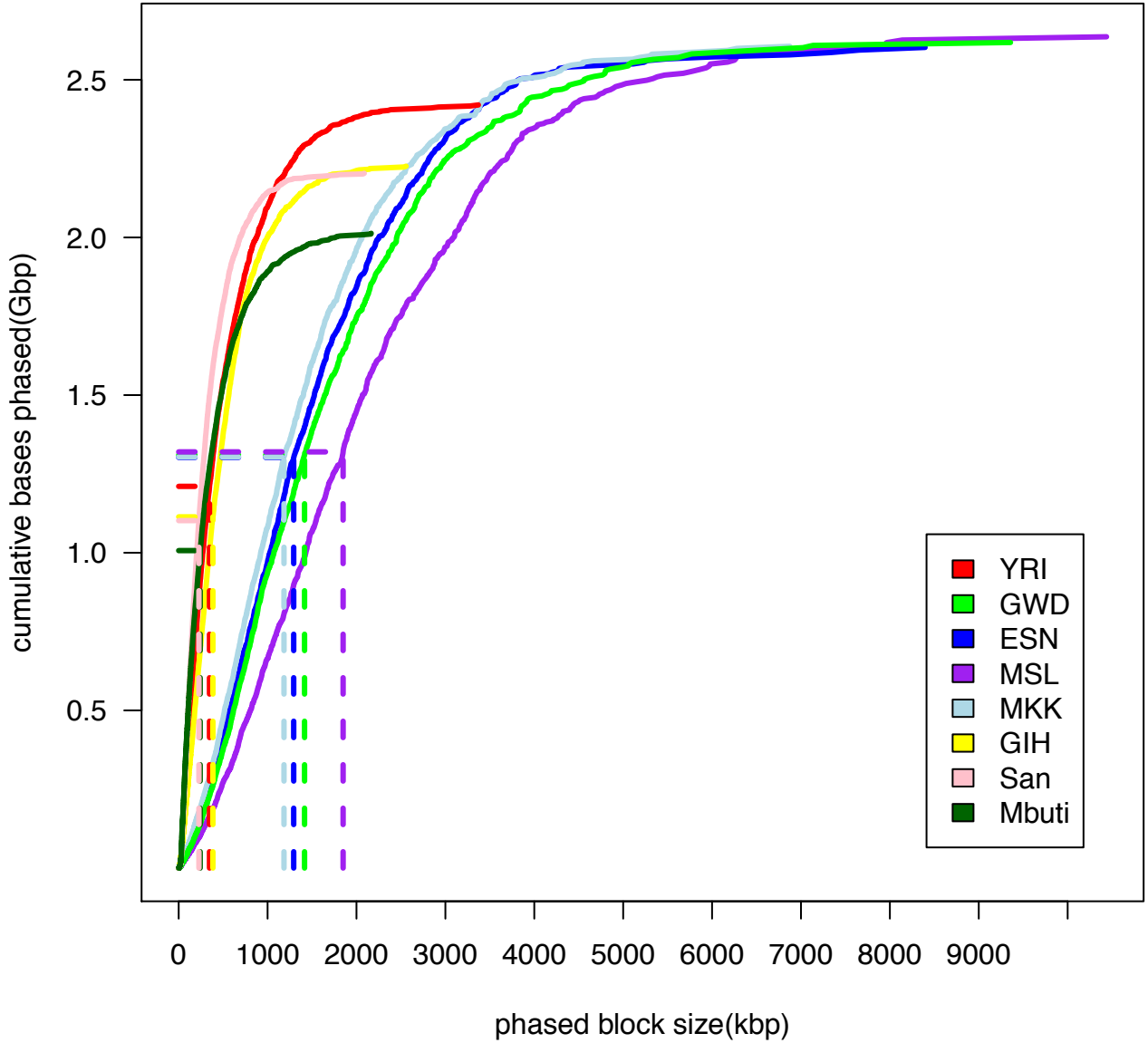
cumulative bases phased(Gbp)
2.5
2.0
1.5
1.0
0.5
0
1000
2000
3000
4000
5000
6000
7000
8000
9000
phased block size(kbp)
YRI
GWD
ESN
MSL
MKK
GIH
San
Mbuti

Figure 2

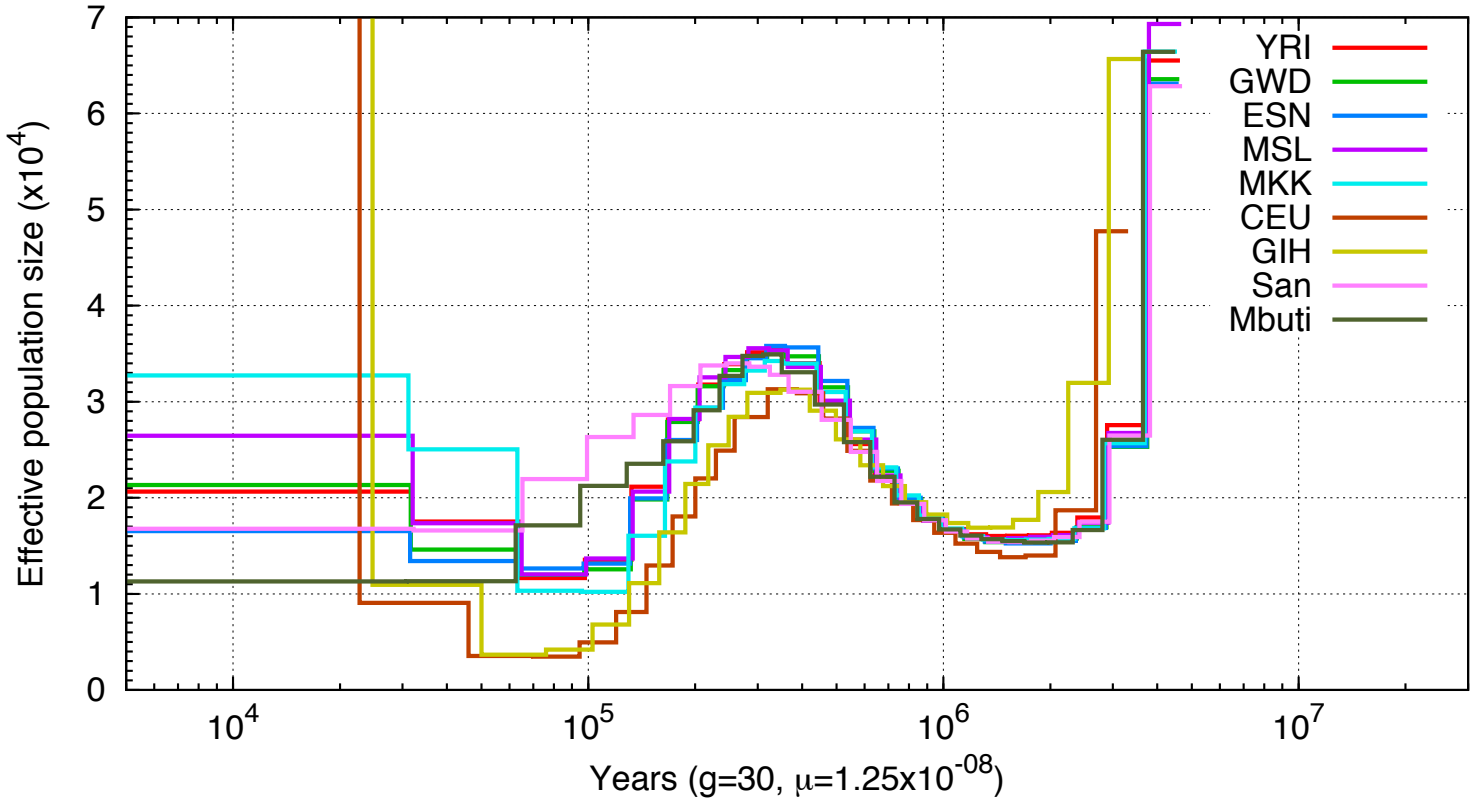
Effective population size (x10^4)
0
1
2
3
4
5
6
7
10^4
10^5
10^6
10^7
Years (g=30, μ=1.25x10^-08)
YRI
GWD
ESN
MSL
MKK
CEU
GIH
San
Mbuti

Figure 3

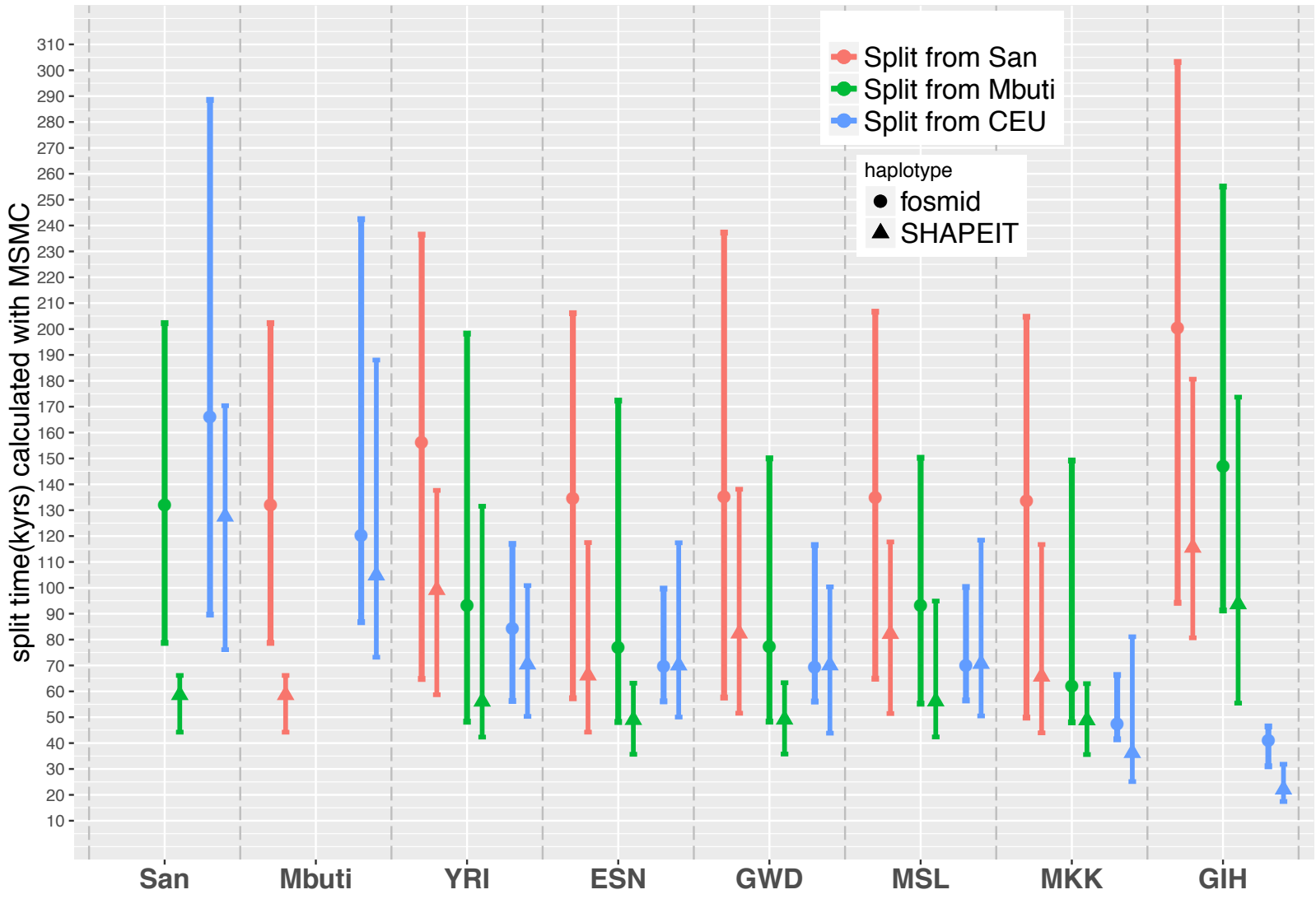
Split from San
Split from Mbuti
Split from CEU
haplotype
fosmid
SHAPEIT
split time(kyrs) calculated with MSMC
310
300
290
280
270
260
250
240
230
220
210
200
190
180
170
160
150
140
130
120
110
100
90
80
70
60
50
40
30
20
10
San
Mbuti
YRI
ESN
GWD
MSL
MKK
GIH

Figure 4

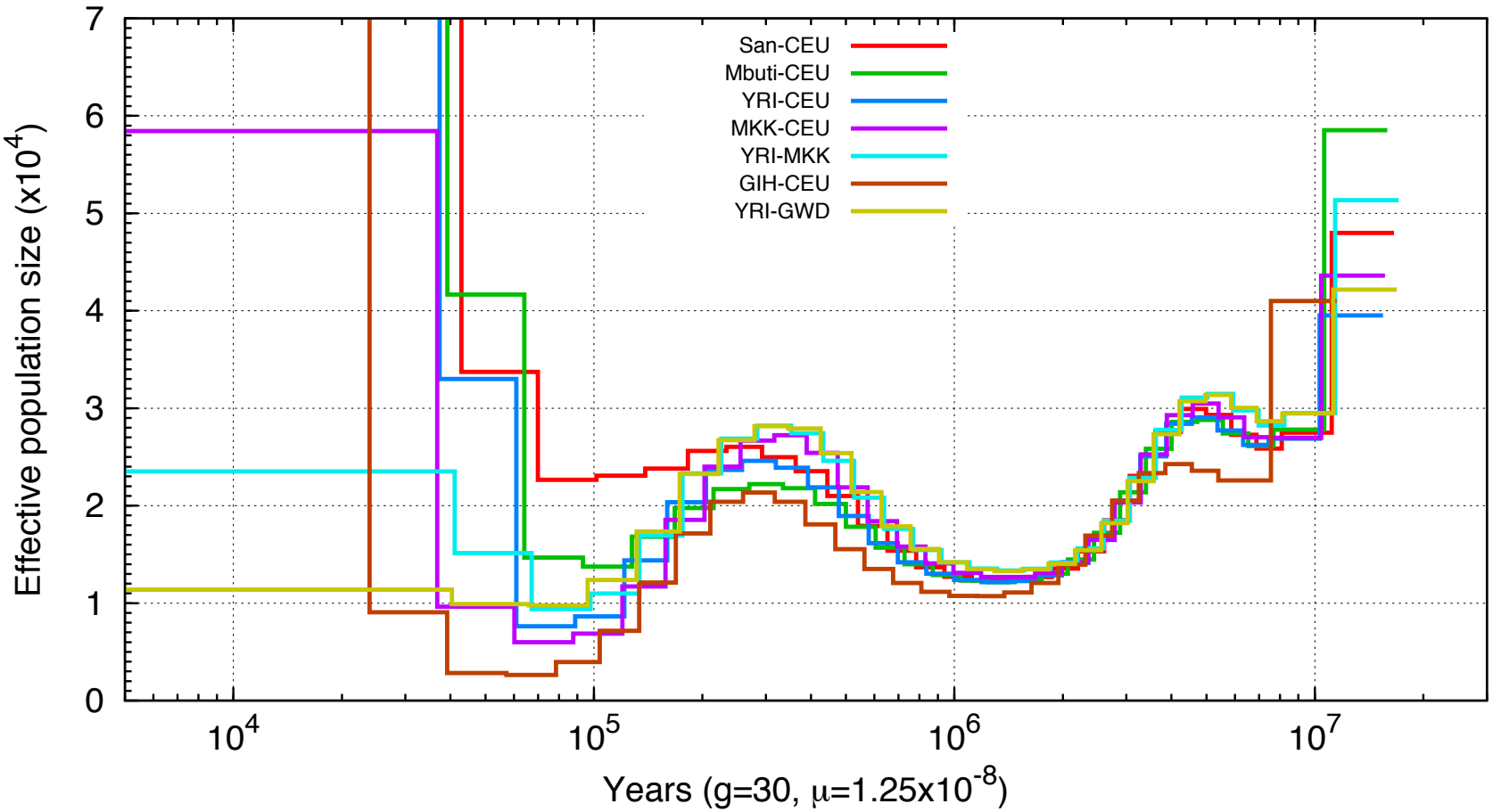
San-CEU
Mbuti-CEU
YRI-CEU
MKK-CEU
YRI-MKK
GIH-CEU
YRI-GWD
Effective population size (x10^4)
0
1
2
3
4
5
6
7
10^4
10^5
10^6
10^7
Years (g=30, μ=1.25x10^-8)

Figure 5

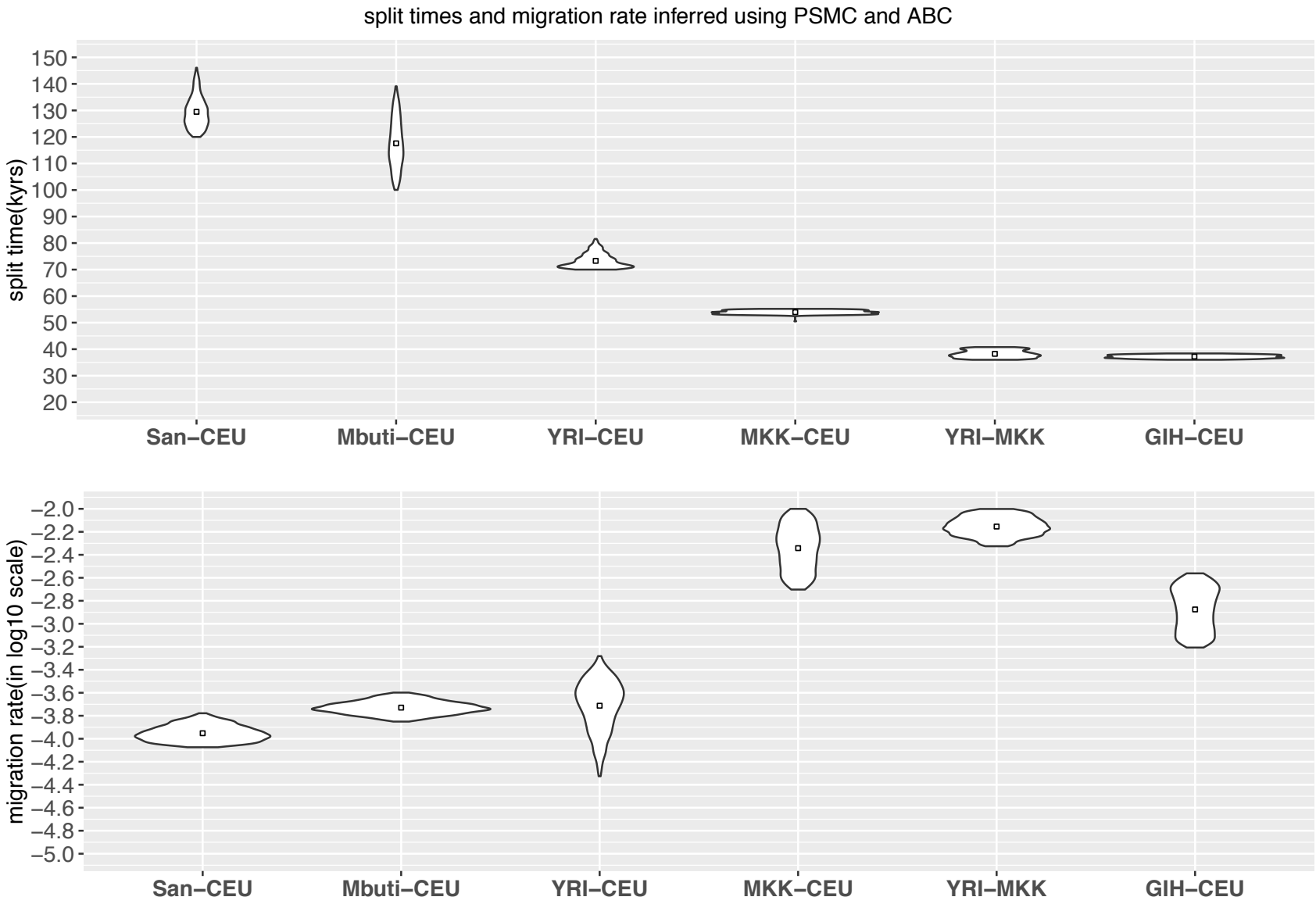
split times and migration rate inferred using PSMC and ABC
split time(kyrs)
150
140
130
120
110
100
90
80
70
60
50
40
30
20
San−CEU
Mbuti−CEU
YRI−CEU
MKK−CEU
YRI−MKK
GIH−CEU
migration rate(in log10 scale)
−2.0
−2.2
−2.4
−2.6
−2.8
−3.0
−3.2
−3.4
−3.6
−3.8
−4.0
−4.2
−4.4
−4.6
−4.8
−5.0
San−CEU
Mbuti−CEU
YRI−CEU
MKK−CEU
YRI−MKK
GIH−CEU

SupFigure 1

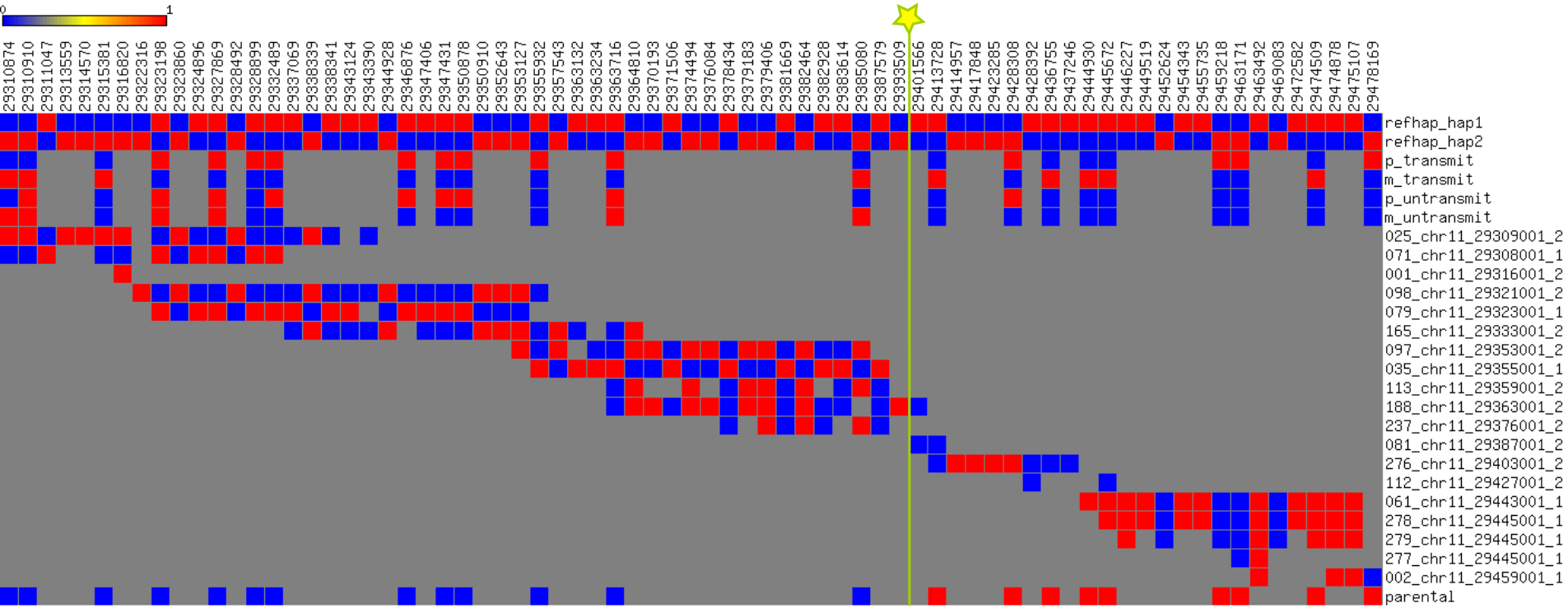
0
1
29310874
29310910
29311047
29313559
29314570
29315381
29316820
29322316
29323198
29323860
29324896
29327869
29328492
29328899
29332489
29337069
29338339
29338341
29343124
29343390
29344928
29346876
29347406
29347431
29350878
29350910
29352643
29353127
29355932
29357543
29363132
29363234
29363716
29364810
29370193
29371506
29374494
29376084
29378434
29379183
29379406
29381669
29382464
29382928
29383614
29385080
29387579
29393509
29401566
29413728
29414957
29417848
29423285
29428308
29428392
29436755
29437246
29444930
29445672
29446227
29449519
29452624
29454343
29455735
29459218
29463171
29463492
29469083
29472582
29474509
29474878
29475107
29478169
refhap_hap1
refhap_hap2
p_transmit
m_transmit
p_untransmit
m_untransmit
025_chr11_29309001_2
071_chr11_29308001_1
001_chr11_29316001_2
098_chr11_29321001_2
079_chr11_29323001_1
165_chr11_29333001_2
097_chr11_29353001_2
035_chr11_29355001_1
113_chr11_29359001_2
188_chr11_29363001_2
237_chr11_29376001_2
081_chr11_29387001_2
276_chr11_29403001_2
112_chr11_29427001_2
061_chr11_29443001_1
278_chr11_29445001_1
279_chr11_29445001_1
277_chr11_29445001_1
002_chr11_29459001_1
parental

SupFigure 2

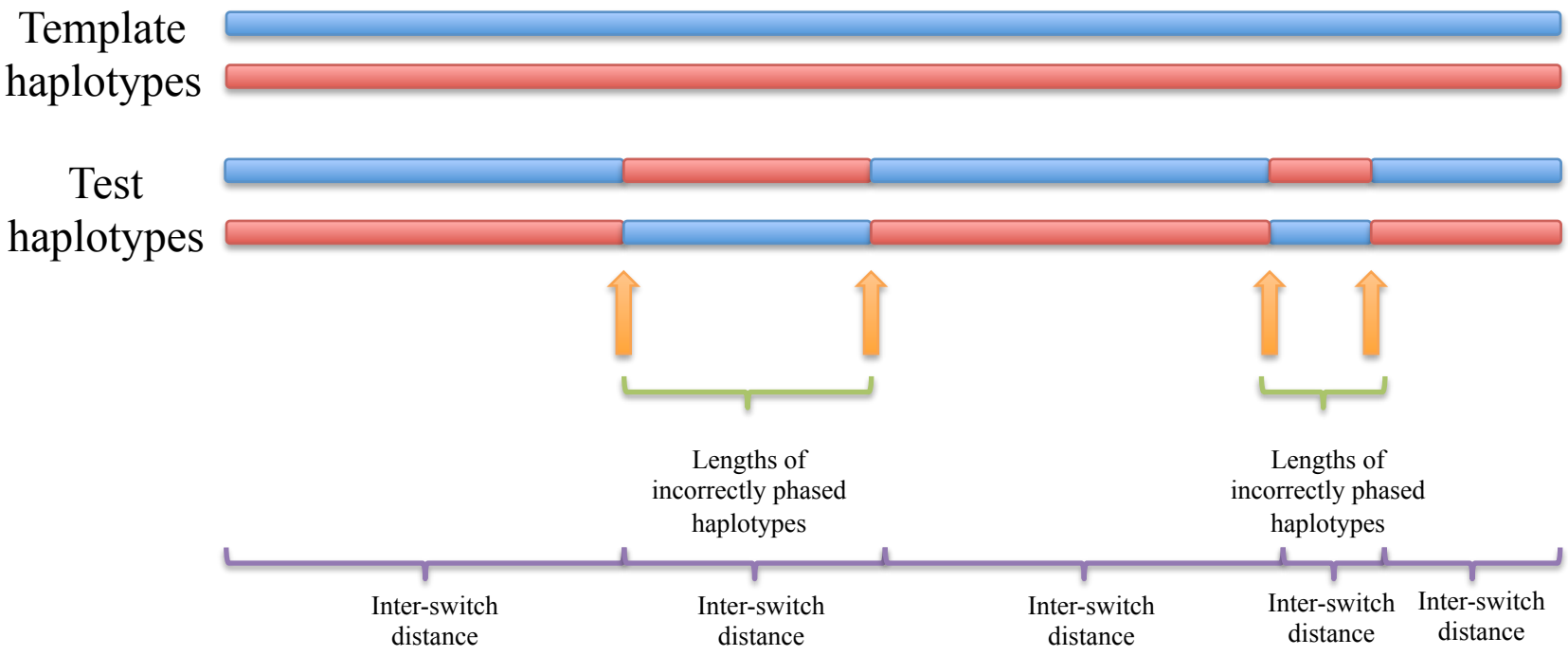
Template haplotypes
Test haplotypes
Lengths of incorrectly phased haplotypes
Lengths of incorrectly phased haplotypes
Inter-switch distance
Inter-switch distance
Inter-switch distance
Inter-switch distance
Inter-switch distance

SupFigure3

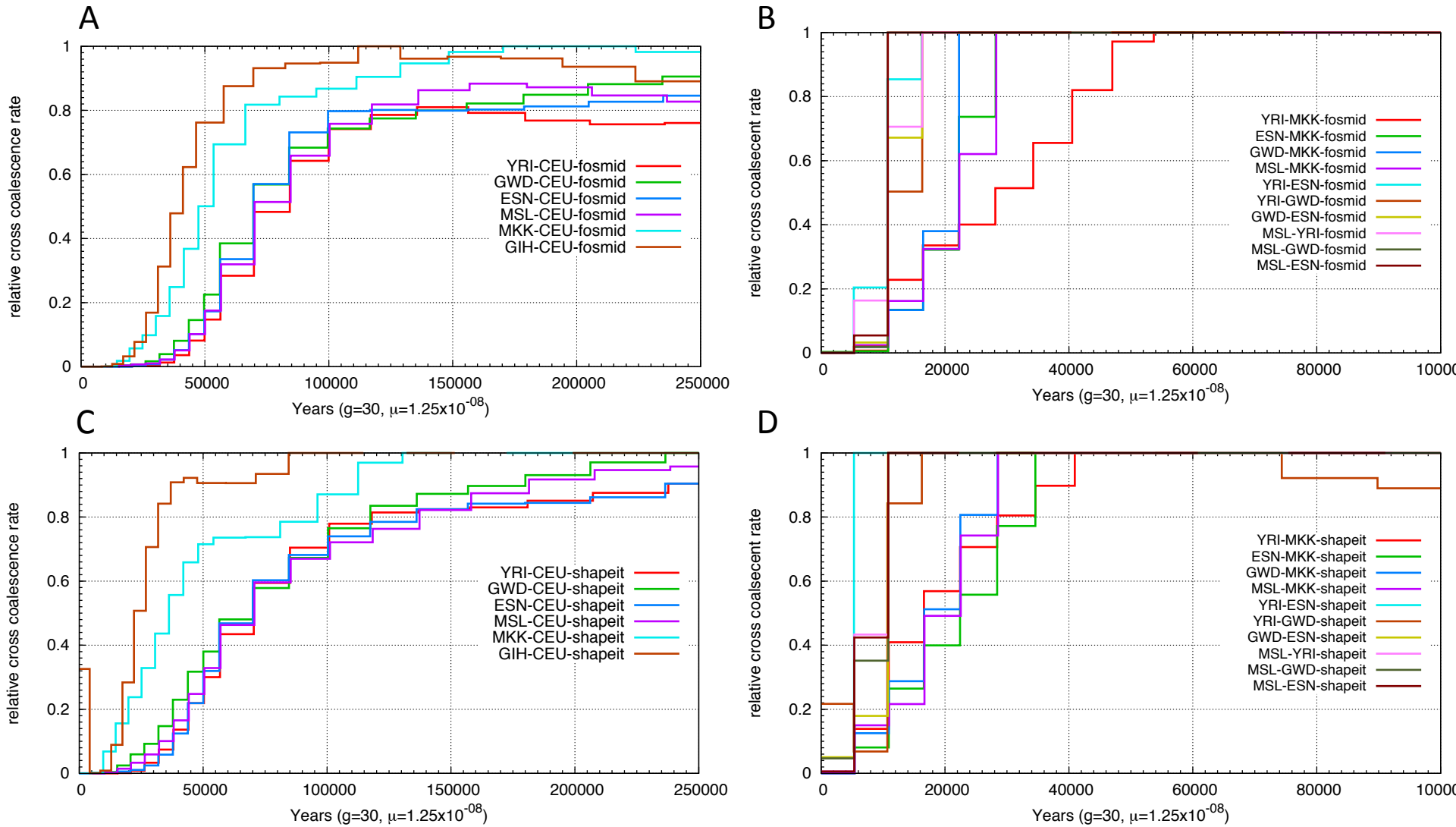
A
relative cross coalescence rate
Years (g=30, μ=1.25x10^-08)
YRI-CEU-fosmid
GWD-CEU-fosmid
ESN-CEU-fosmid
MSL-CEU-fosmid
MKK-CEU-fosmid
GIH-CEU-fosmid
B
relative cross coalsecent rate
Years (g=30, μ=1.25x10^-08)
YRI-MKK-fosmid
ESN-MKK-fosmid
GWD-MKK-fosmid
MSL-MKK-fosmid
YRI-ESN-fosmid
YRI-GWD-fosmid
GWD-ESN-fosmid
MSL-YRI-fosmid
MSL-GWD-fosmid
MSL-ESN-fosmid
C
relative cross coalescence rate
Years (g=30, μ=1.25x10^-08)
YRI-CEU-shapeit
GWD-CEU-shapeit
ESN-CEU-shapeit
MSL-CEU-shapeit
MKK-CEU-shapeit
GIH-CEU-shapeit
D
relative cross coalsecent rate
Years (g=30, μ=1.25x10^-08)
YRI-MKK-shapeit
ESN-MKK-shapeit
GWD-MKK-shapeit
MSL-MKK-shapeit
YRI-ESN-shapeit
YRI-GWD-shapeit
GWD-ESN-shapeit
MSL-YRI-shapeit
MSL-GWD-shapeit
MSL-ESN-shapeit

SupFigure3

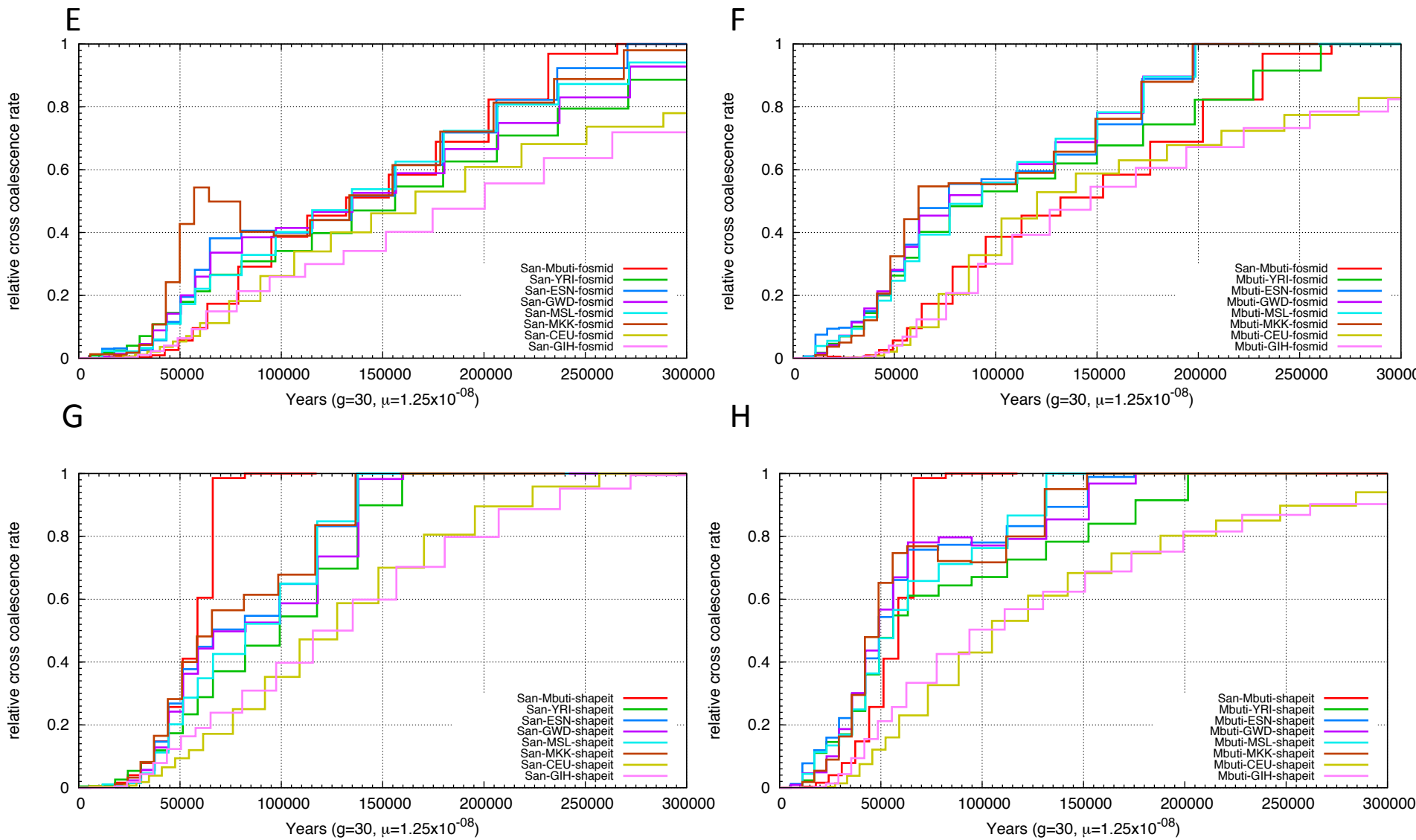
E
F
G
H
relative cross coalescence rate
Years (g=30, μ=1.25x10^-08)
0
0.2
0.4
0.6
0.8
1
0
50000
100000
150000
200000
250000
300000
San-Mbuti-fosmid
San-YRI-fosmid
San-ESN-fosmid
San-GWD-fosmid
San-MSL-fosmid
San-MKK-fosmid
San-CEU-fosmid
San-GIH-fosmid
Mbuti-YRI-fosmid
Mbuti-ESN-fosmid
Mbuti-GWD-fosmid
Mbuti-MSL-fosmid
Mbuti-MKK-fosmid
Mbuti-CEU-fosmid
Mbuti-GIH-fosmid
San-Mbuti-shapeit
San-YRI-shapeit
San-ESN-shapeit
San-GWD-shapeit
San-MSL-shapeit
San-MKK-shapeit
San-CEU-shapeit
San-GIH-shapeit
Mbuti-YRI-shapeit
Mbuti-ESN-shapeit
Mbuti-GWD-shapeit
Mbuti-MSL-shapeit
Mbuti-MKK-shapeit
Mbuti-CEU-shapeit
Mbuti-GIH-shapeit

SupFigure 4

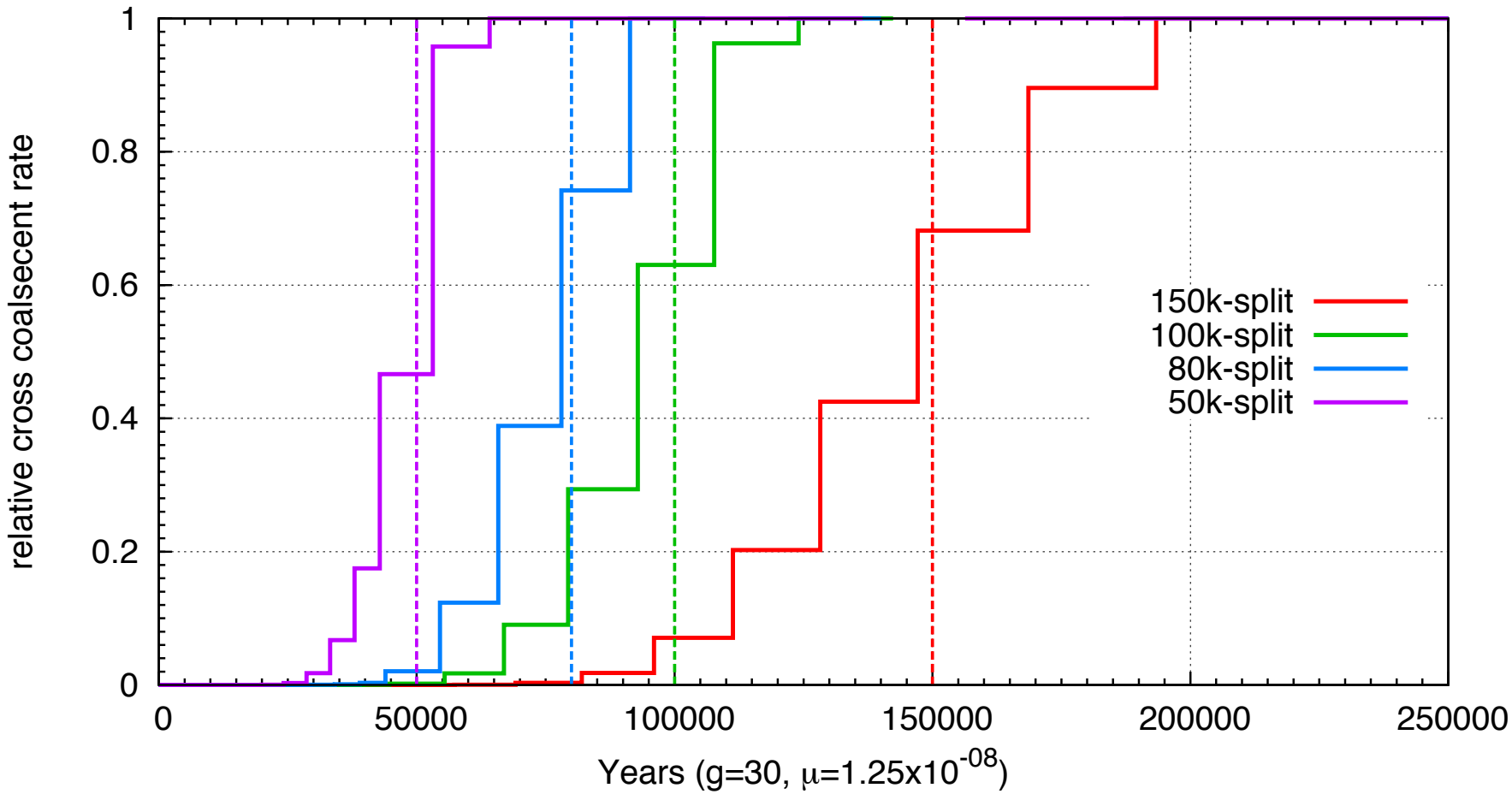
relative cross coalsecent rate
1
0.8
0.6
0.4
0.2
0
0
50000
100000
150000
200000
250000
Years (g=30, μ=1.25x10^-08)
150k-split
100k-split
80k-split
50k-split

SupFigure5

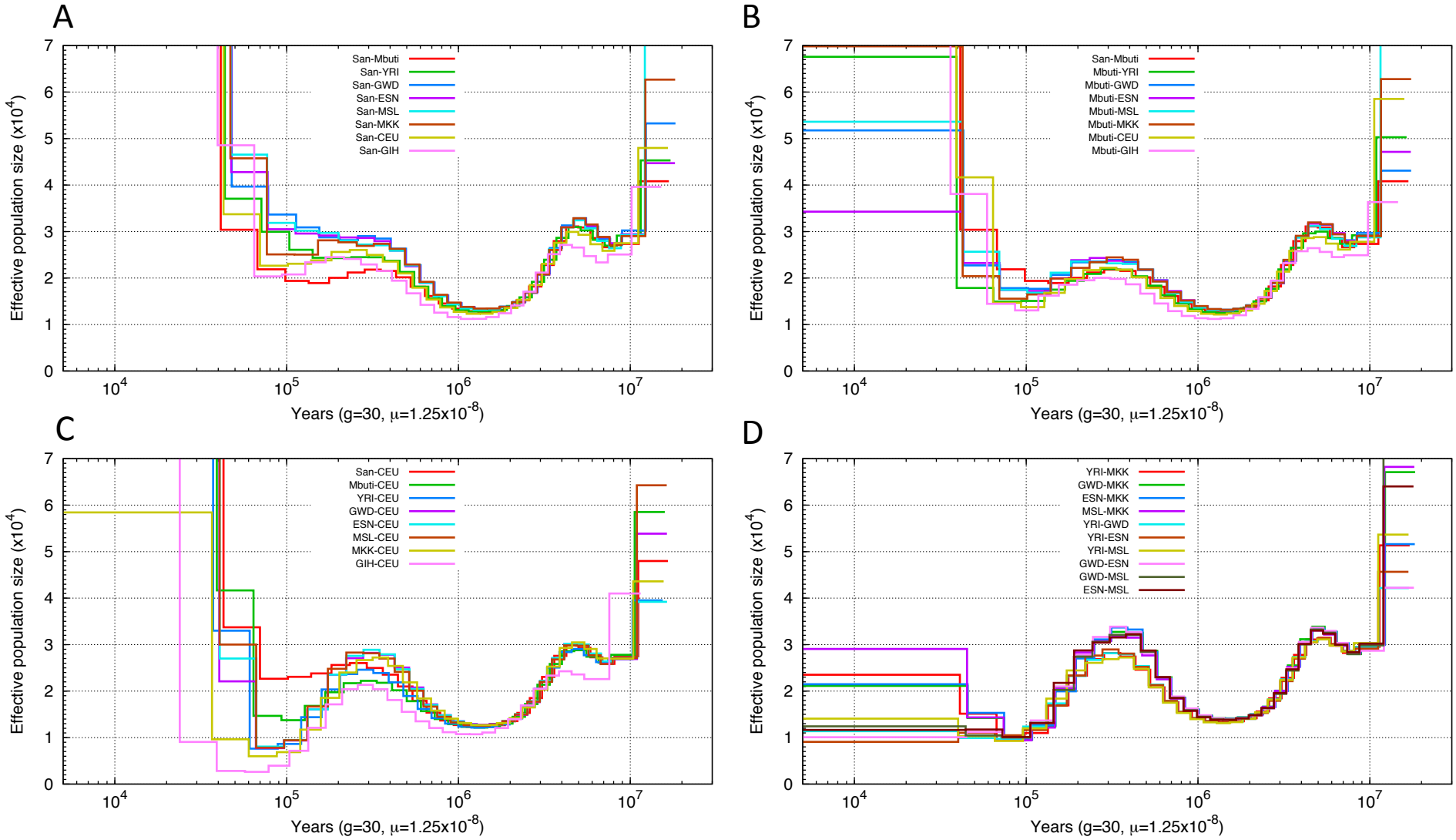
A
B
C
D
Effective population size (x10^4)
Years (g=30, μ=1.25x10^-8)
San-Mbuti
San-YRI
San-GWD
San-ESN
San-MSL
San-MKK
San-CEU
San-GIH
Mbuti-YRI
Mbuti-GWD
Mbuti-ESN
Mbuti-MSL
Mbuti-MKK
Mbuti-CEU
Mbuti-GIH
Mbuti-CEU
YRI-CEU
GWD-CEU
ESN-CEU
MSL-CEU
MKK-CEU
GIH-CEU
YRI-MKK
GWD-MKK
ESN-MKK
MSL-MKK
YRI-GWD
YRI-ESN
YRI-MSL
GWD-ESN
GWD-MSL
ESN-MSL

SupFigure 6

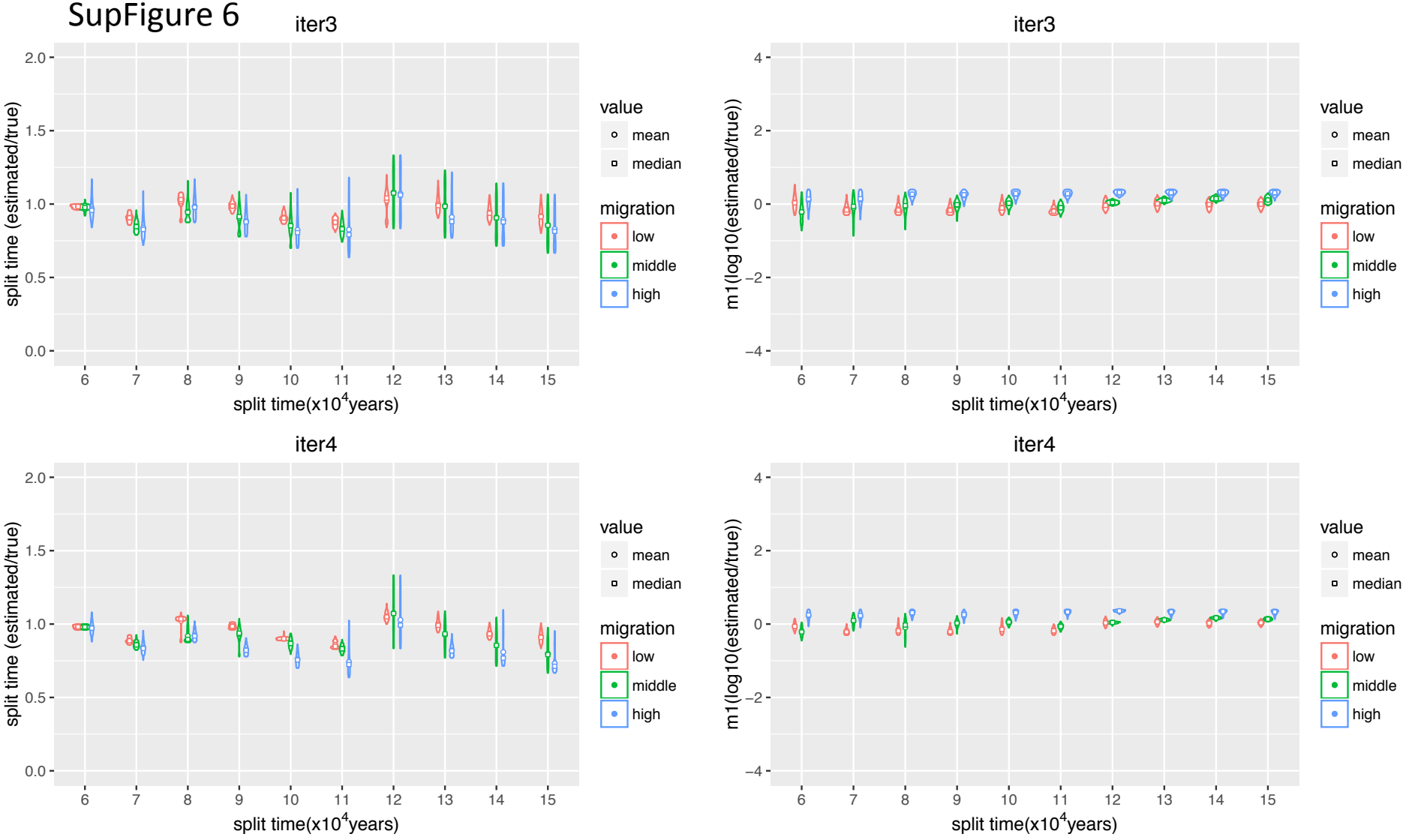
iter3
iter3
iter4
iter4
split time (estimated/true)
m1(log10(estimated/true))
split time(x10^4years)
value
mean
median
migration
low
middle
high

SupFigure7

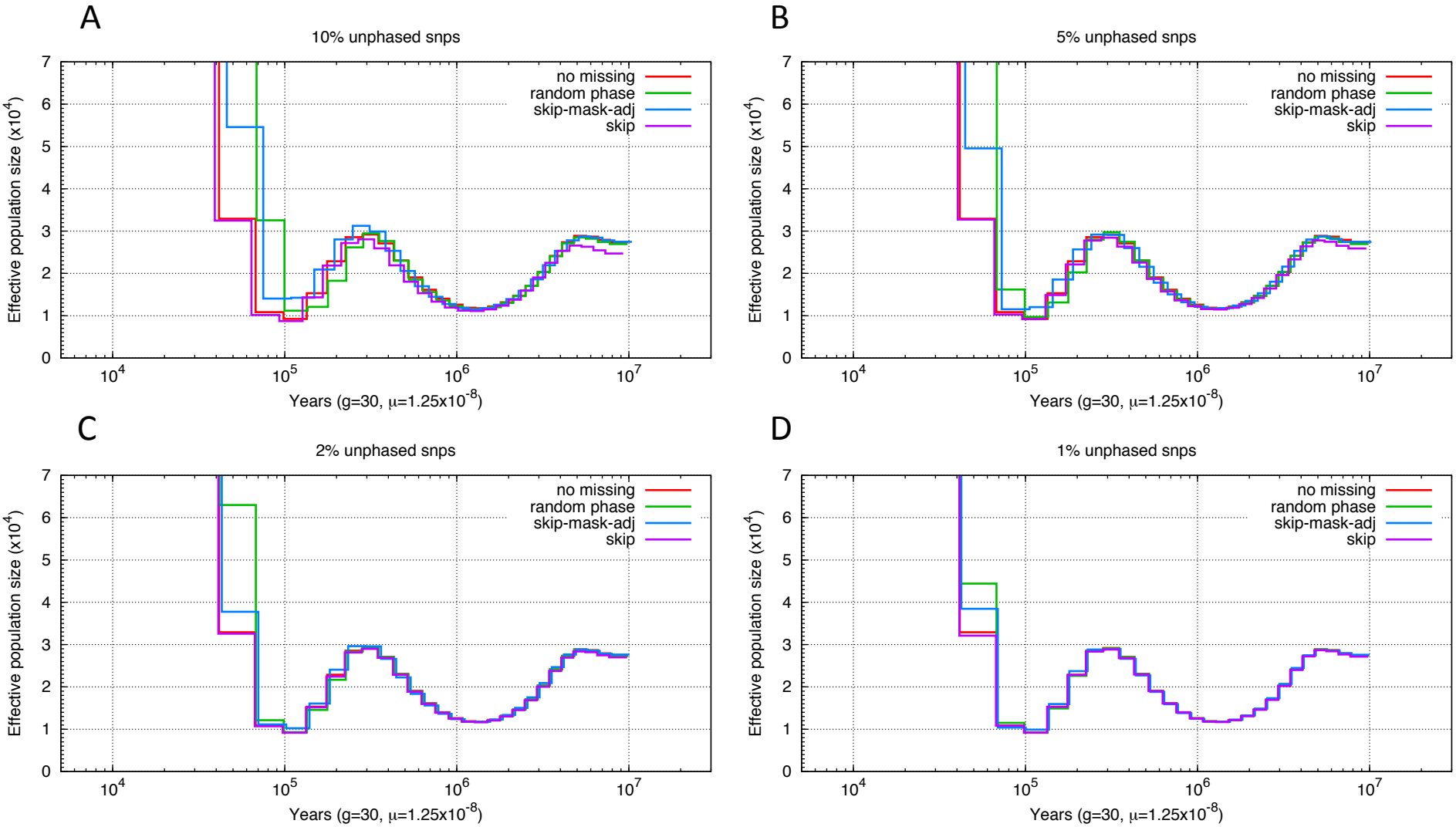
A
10% unphased snps
B
5% unphased snps
C
2% unphased snps
D
1% unphased snps
no missing
random phase
skip-mask-adj
skip
Effective population size (x10^4)
Years (g=30, μ=1.25x10^-8)
0
1
2
3
4
5
6
7
10^4
10^5
10^6
10^7

SupFigure8

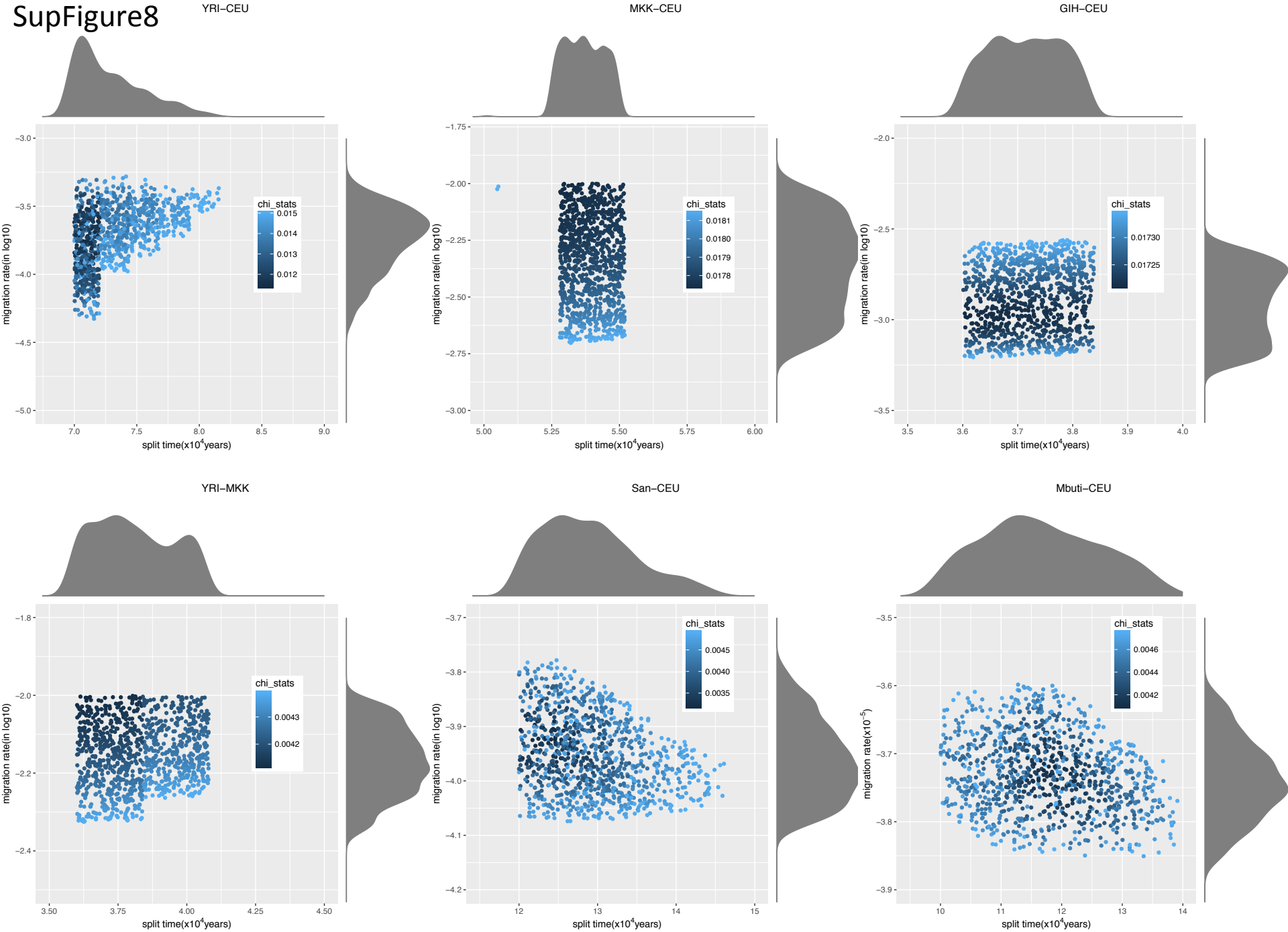
YRI–CEU
MKK–CEU
GIH–CEU
YRI–MKK
San–CEU
Mbuti–CEU
chi_stats
0.015
0.014
0.013
0.012
0.0181
0.0180
0.0179
0.0178
0.01730
0.01725
0.0043
0.0042
0.0045
0.0040
0.0035
0.0046
0.0044
0.0042
migration rate(in log10)
migration rate(x10^-5)
split time(x10^4years)

SupFigure 9

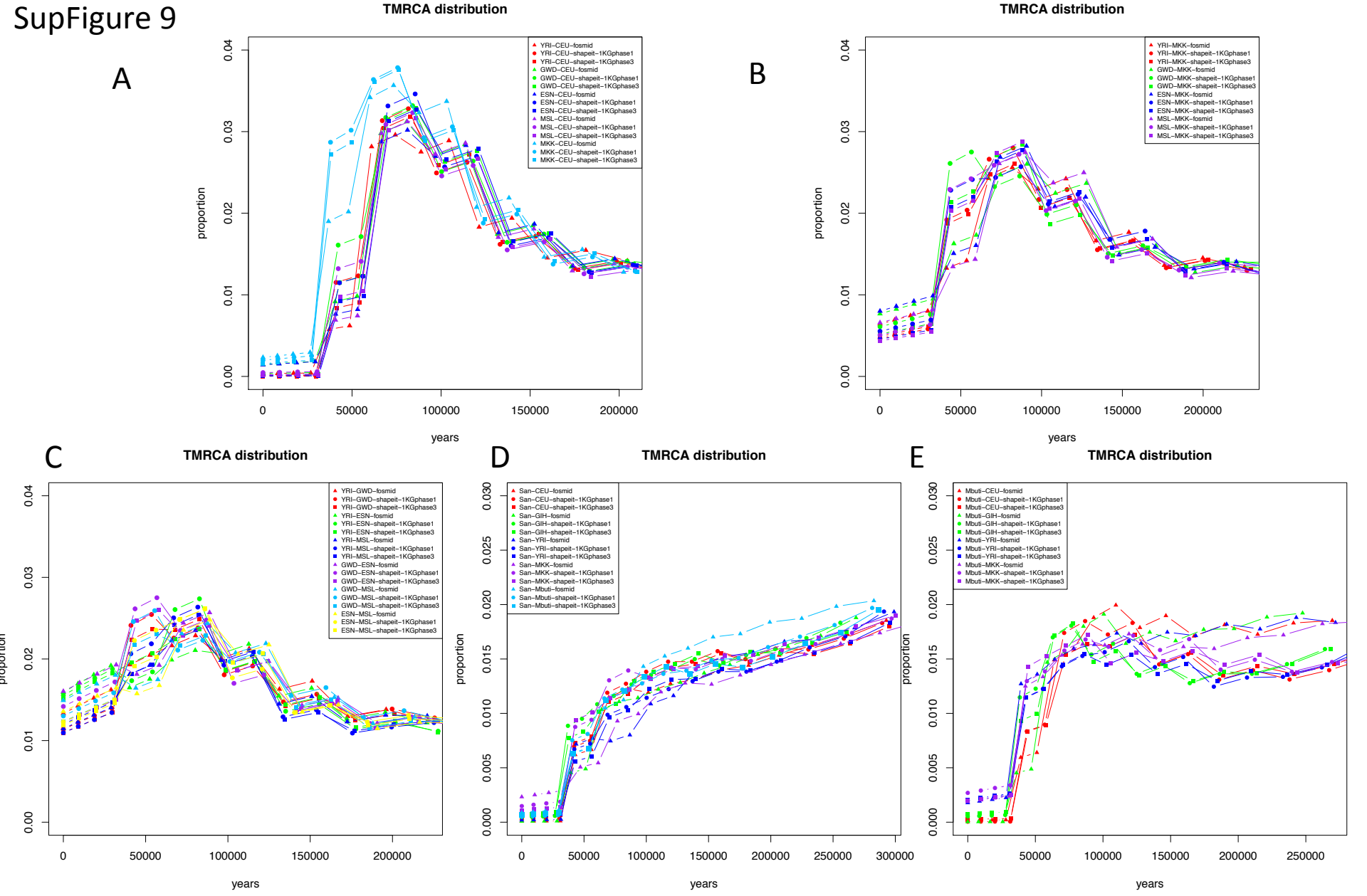
A
TMRCA distribution
proportion
years
YRI–CEU–fosmid
YRI–CEU–shapeit–1KGphase1
YRI–CEU–shapeit–1KGphase3
GWD–CEU–fosmid
GWD–CEU–shapeit–1KGphase1
GWD–CEU–shapeit–1KGphase3
ESN–CEU–fosmid
ESN–CEU–shapeit–1KGphase1
ESN–CEU–shapeit–1KGphase3
MSL–CEU–fosmid
MSL–CEU–shapeit–1KGphase1
MSL–CEU–shapeit–1KGphase3
MKK–CEU–fosmid
MKK–CEU–shapeit–1KGphase1
MKK–CEU–shapeit–1KGphase3
B
TMRCA distribution
proportion
years
YRI–MKK–fosmid
YRI–MKK–shapeit–1KGphase1
YRI–MKK–shapeit–1KGphase3
GWD–MKK–fosmid
GWD–MKK–shapeit–1KGphase1
GWD–MKK–shapeit–1KGphase3
ESN–MKK–fosmid
ESN–MKK–shapeit–1KGphase1
ESN–MKK–shapeit–1KGphase3
MSL–MKK–fosmid
MSL–MKK–shapeit–1KGphase1
MSL–MKK–shapeit–1KGphase3
C
TMRCA distribution
proportion
years
YRI–GWD–fosmid
YRI–GWD–shapeit–1KGphase1
YRI–GWD–shapeit–1KGphase3
YRI–ESN–fosmid
YRI–ESN–shapeit–1KGphase1
YRI–ESN–shapeit–1KGphase3
YRI–MSL–fosmid
YRI–MSL–shapeit–1KGphase1
YRI–MSL–shapeit–1KGphase3
GWD–ESN–fosmid
GWD–ESN–shapeit–1KGphase1
GWD–ESN–shapeit–1KGphase3
GWD–MSL–fosmid
GWD–MSL–shapeit–1KGphase1
GWD–MSL–shapeit–1KGphase3
ESN–MSL–fosmid
ESN–MSL–shapeit–1KGphase1
ESN–MSL–shapeit–1KGphase3
D
TMRCA distribution
proportion
years
San–CEU–fosmid
San–CEU–shapeit–1KGphase1
San–CEU–shapeit–1KGphase3
San–GIH–fosmid
San–GIH–shapeit–1KGphase1
San–GIH–shapeit–1KGphase3
San–YRI–fosmid
San–YRI–shapeit–1KGphase1
San–YRI–shapeit–1KGphase3
San–MKK–fosmid
San–MKK–shapeit–1KGphase1
San–MKK–shapeit–1KGphase3
San–Mbuti–fosmid
San–Mbuti–shapeit–1KGphase1
San–Mbuti–shapeit–1KGphase3
E
TMRCA distribution
proportion
years
Mbuti–CEU–fosmid
Mbuti–CEU–shapeit–1KGphase1
Mbuti–CEU–shapeit–1KGphase3
Mbuti–GIH–fosmid
Mbuti–GIH–shapeit–1KGphase1
Mbuti–GIH–shapeit–1KGphase3
Mbuti–YRI–fosmid
Mbuti–YRI–shapeit–1KGphase1
Mbuti–YRI–shapeit–1KGphase3
Mbuti–MKK–fosmid
Mbuti–MKK–shapeit–1KGphase1
Mbuti–MKK–shapeit–1KGphase3

SupFigure 10

A

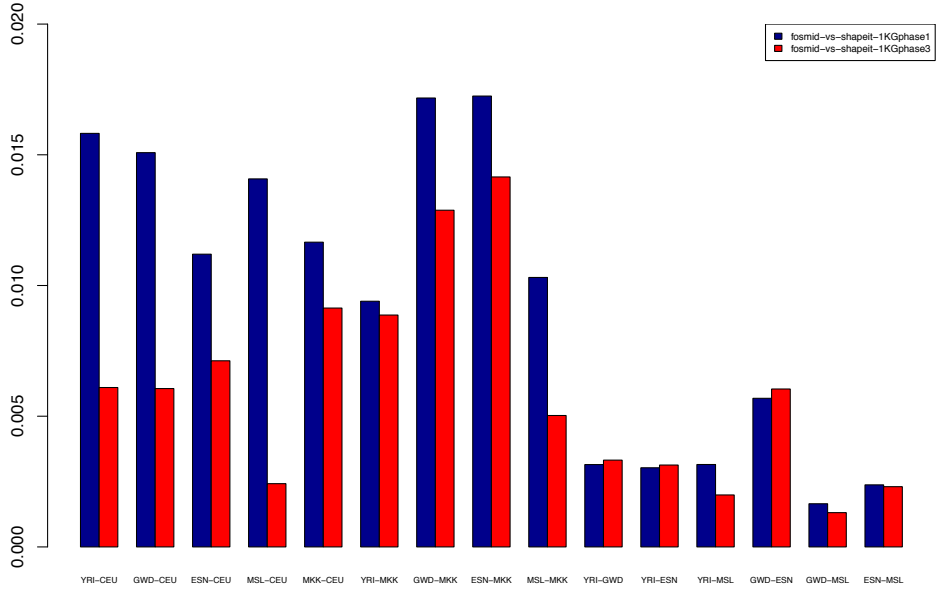

B

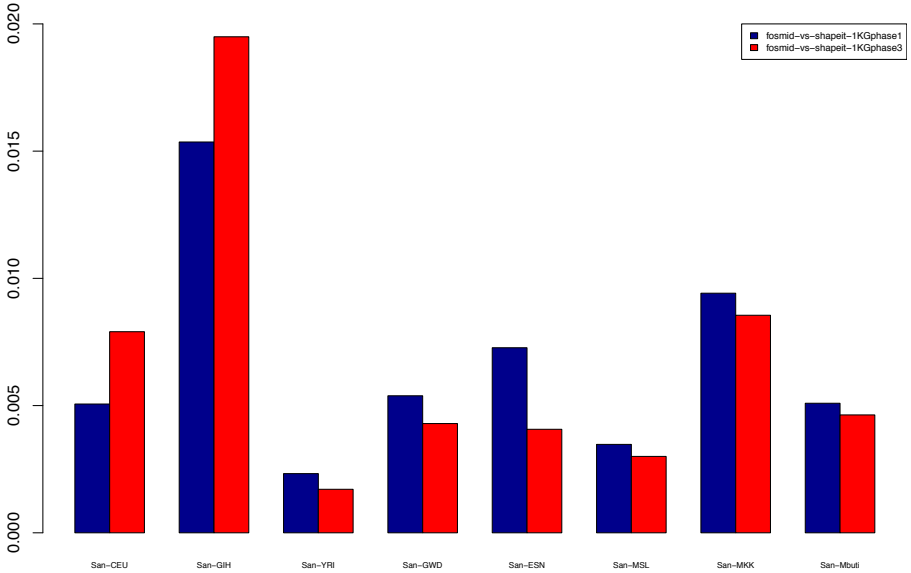

C

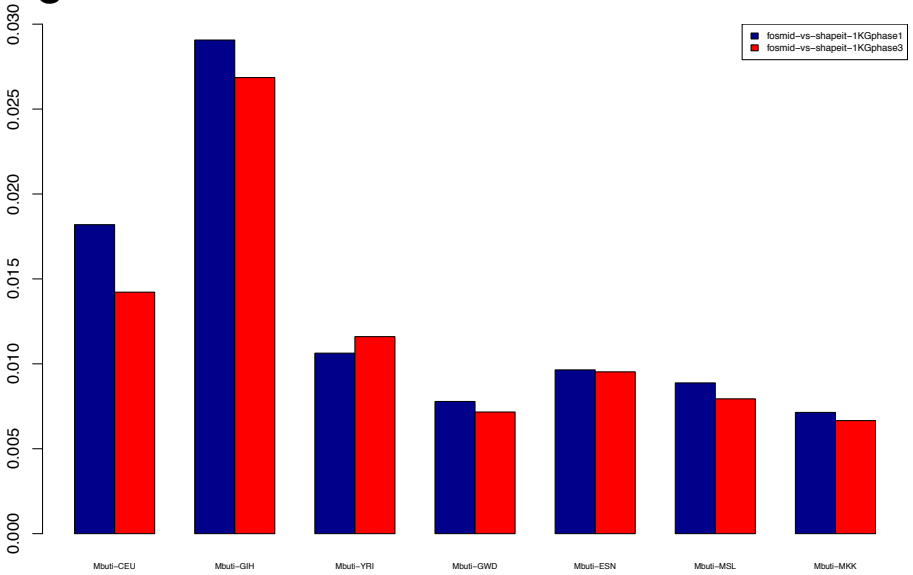

SupFigure 11

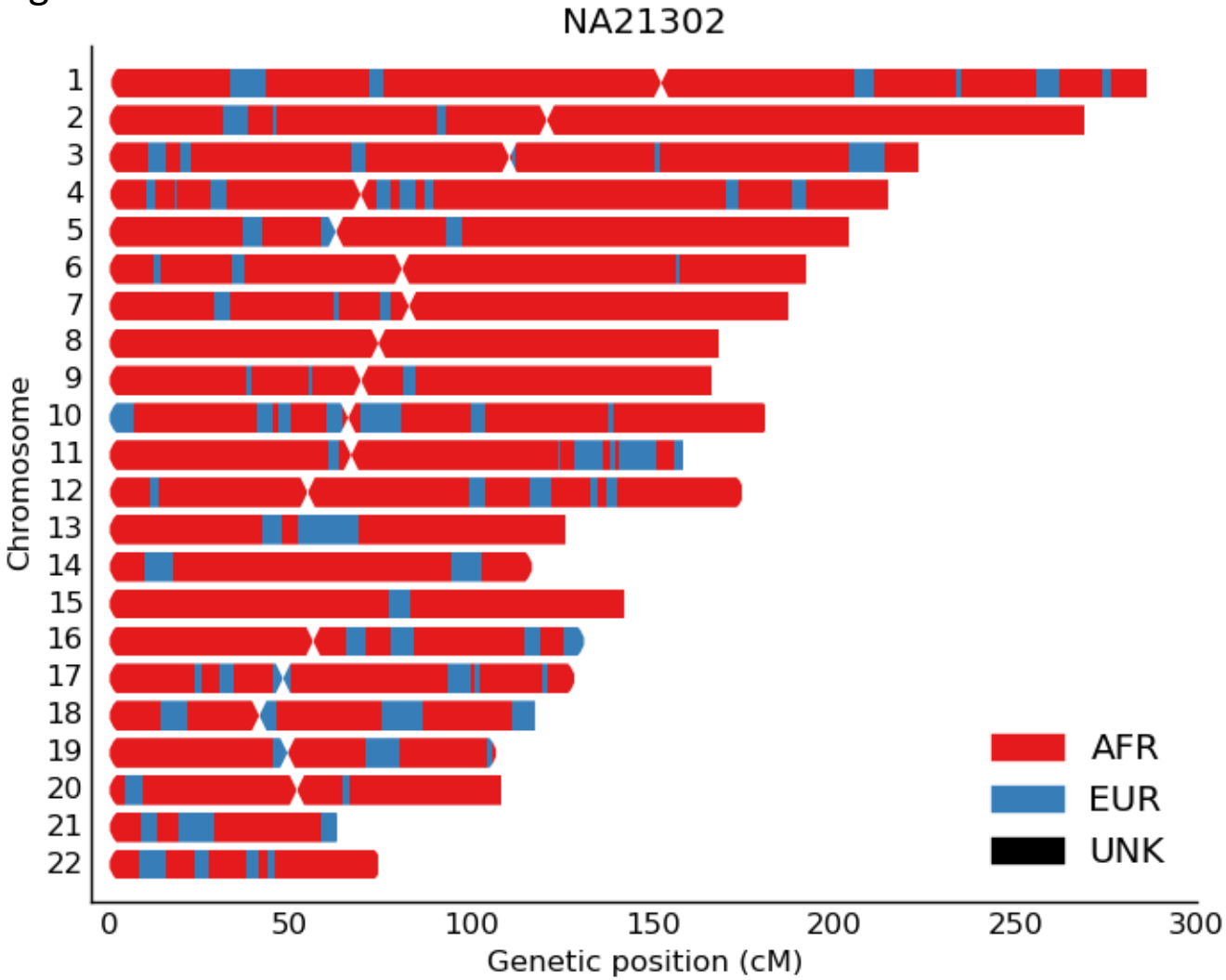

SupFigure 12

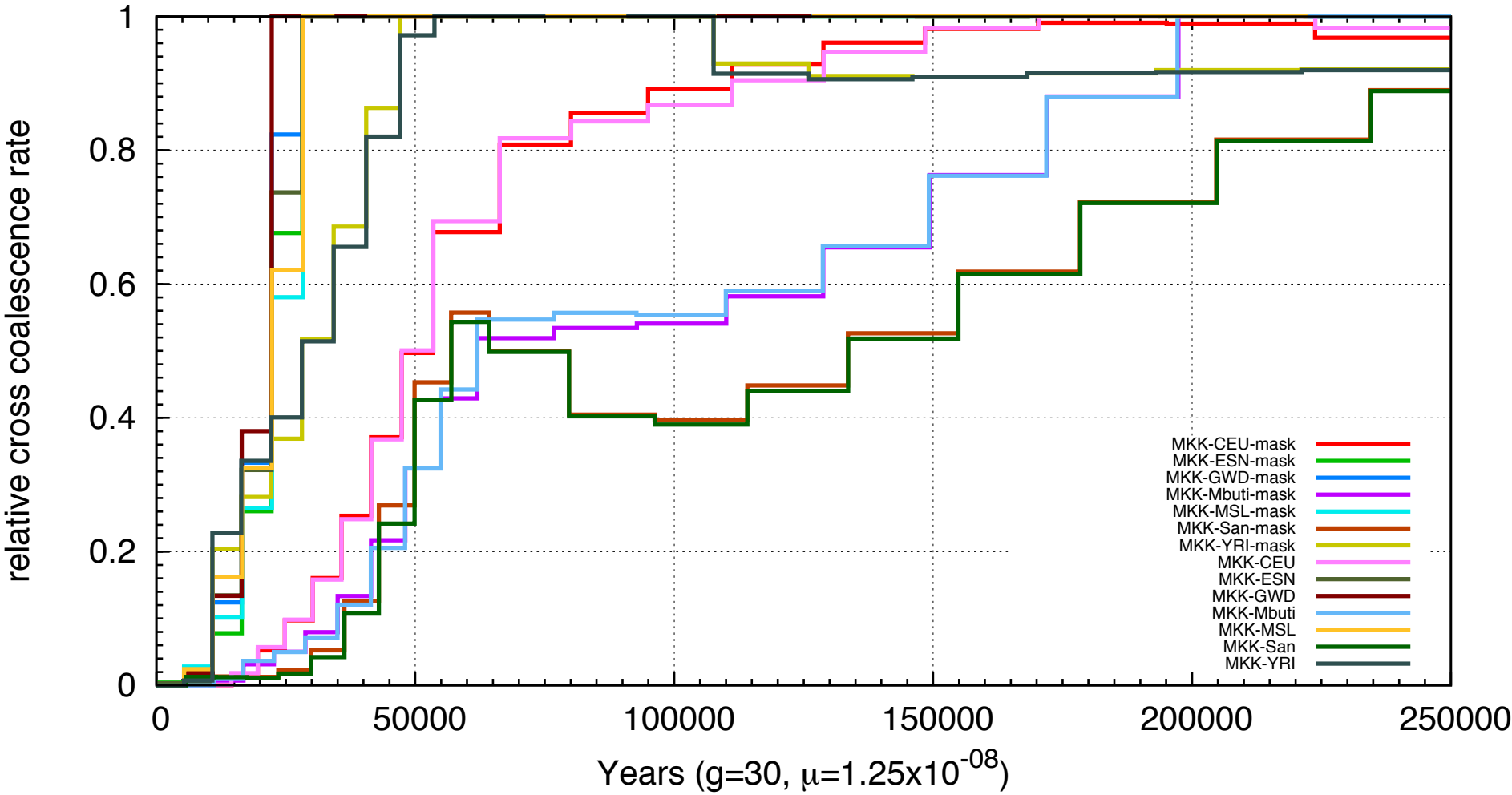
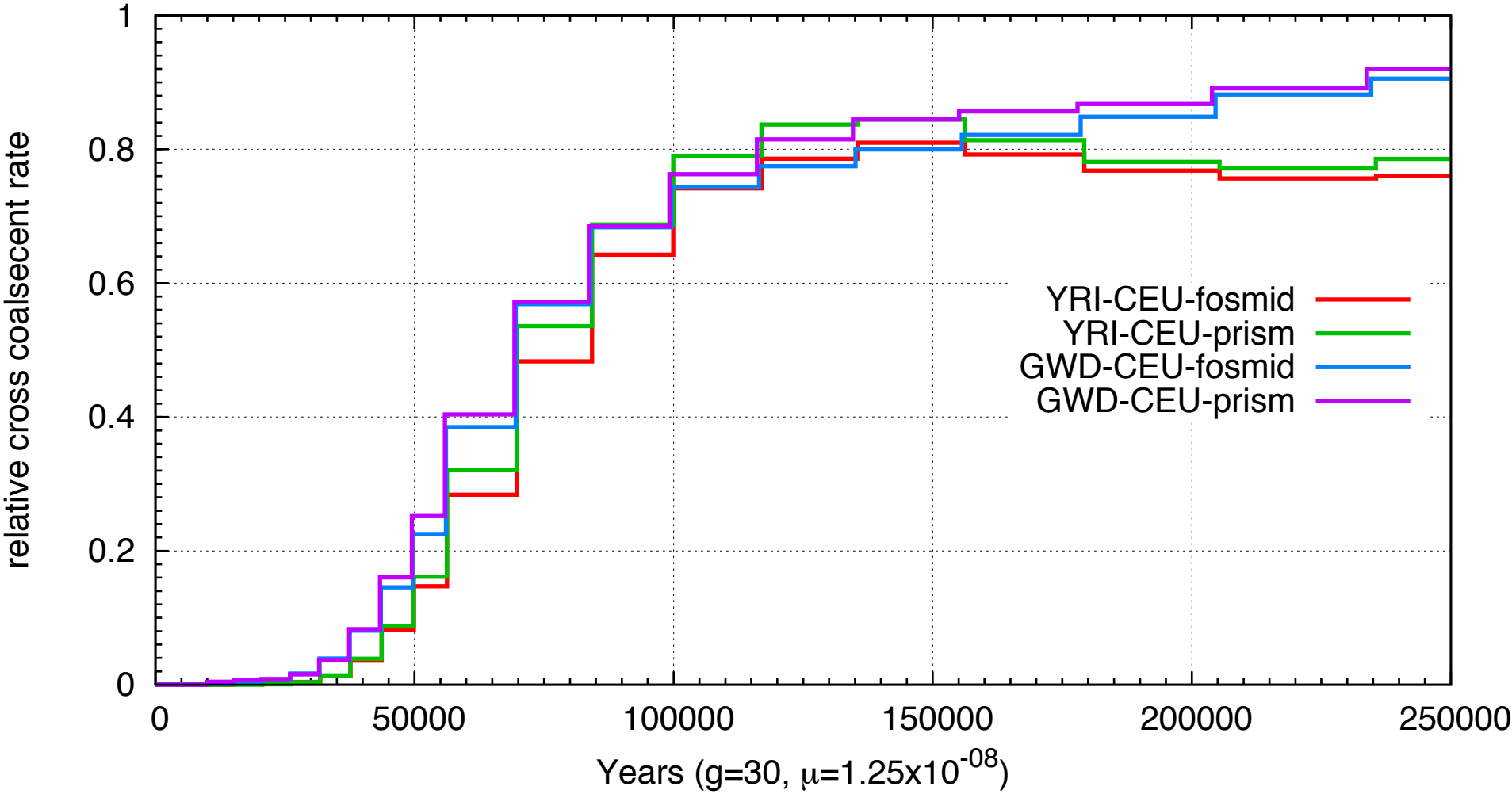
SupFigure 13